ARTICLE

Mechanically interlocked molecules in metal-organic frameworks

Adrian Saura-Sanmartin,[a] Aurelia Pastor,[a] Alberto Martinez-Cuezva,[a] Guillermo Cutillas-Font,[a] Mateo Alajarin[a] and Jose Berna*[a]

Received 00th January 20xx,
Accepted 00th January 20xx

DOI: 10.1039/x0xx00000x

Mechanically interlocked molecules (MIMs) have great potential in the development of molecular machinery due to their intercomponent dynamics. The incorporation of these molecules in a condensed phase allows to take advantage of the control of the motion of the components at the macroscopic level. Metal-organic frameworks (MOFs) are postulated as ideal supports for intertwined molecules. This review covers the chemistry of the mechanical bond incorporated into metal-organic frameworks since the seminal works to the latest published advances. We first describe some fundamental concepts of MIMs and MOFs. Next, we summarize the advances in the incorporation of rotaxanes and catenanes inside MOF matrices. Finally, we continue by showing the study of the rotaxane dynamics in MOFs and the operation of some stimuli-responsives MIMs within MOFs. In addition to highlight some selected examples, we offer a critical opinion on the state of the art of this research field, remarking the key points on which the future of these systems should be focused on.

1. Introduction

Metal-organic frameworks (MOFs)[1–5] constitute a type of highly stable porous materials with several advantages over the conventional analogous such as zeolites.[6] These materials are made from organic linkers coordinated to metal ions, forming a well-ordered crystalline array. Thus, their great design versatility, with an uncountable number of possible combinations, enables the easy control of its pore size and internal surface area.[7]

The chemistry of MOFs has attracted the attention of numerous chemists thanks to the possibility of preparing infinite structures from a great number of metal precursors and a wide range of organic ligands, including commercial ones or synthesized in the laboratory. The ability of the metal ions to show variable coordination numbers and geometries is a major advantage in the preparation of MOFs, in which metal cores and organic struts are linked in specific positions.[8] In order to block metal ions in the appropriate positions and, thus, to facilitate the control in the preparation of specific structures, metal complexes and clusters, named as Secondary Building Units (SBUs), have been commonly used in the systematization of the synthesis of MOFs.[9] Typically, the combination of a particular organic ligand containing carboxyl functional groups and a SBU determines the structure of the resulting MOF (Fig. 1). Therefore, the design of the morphology of the structure, as well as the pore size, can be easily programmed. This fact has resulted in numerous applications of these systems, such as gas adsorption,[10] heterogeneous catalysis[11] or water harvesting.[12,13] One of the main trends for carrying out novel research on MOFs is focused on the preparation of materials with advanced functionalities.

Progress in the chemistry of MOFs ran parallel with the development of novel mechanically interlocked molecules (MIMs).[14] These entangled compounds are constituted by at least two components which are not covalently linked, but there is a physical bond that keep them intertwined one another, stabilized by non-covalent interactions such as van der Waals forces, aromatics interactions or hydrogen bonds. The union between the components is known as mechanical bond.[15] The synthesis of MIMs, mainly rotaxanes and catenanes, and the switching of their intercomponent dynamics is a topic of great interest nowadays. A wide range of supramolecular systems take advantage of the chemistry of the mechanical bond. Different applications of these interlocked molecules have been developed, from which the design of sophisticated molecular machines performing a proper switching as a response to an external stimulus should be highlighted.[15–18]

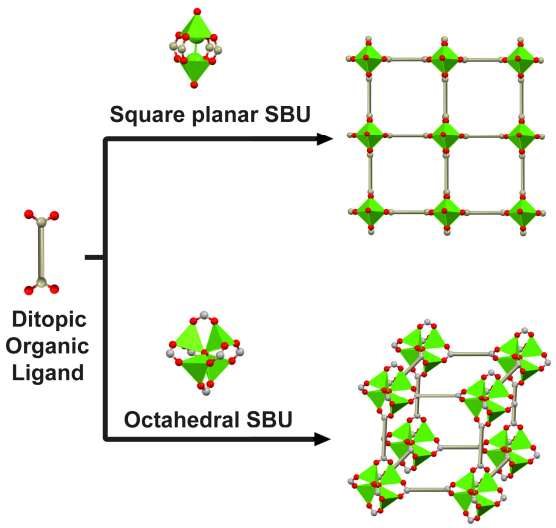

Fig. 1 Use of a ditopic organic ligand with two SBUs, $M_2(O_2CR)_4L_2$ having a planar square coordination geometry and $M_4O(O_2CR)_6$ having an octahedral coordination geometry, for the building of 2D- and 3D-MOFs. M = transition metal (e.g. Cu, Zn) and L = axial ligand (e.g. H_2O).

[a] Departamento de Química Orgánica, Facultad de Química, Regional Campus of International Excellence "Campus Mare Nostrum", Universidad de Murcia, E-30100, Murcia, Spain. E-mail: ppberna@um.es.

Adrian Saura-Sanmartin

Adrian Saura-Sanmartin obtained his degree in Chemistry at the Universidad de Murcia in 2015. In 2016, he obtained his Master degree in Organic Chemistry at the Universidad Complutense de Madrid. In 2018, he was awarded with a Fundacion Seneca predoctoral contract. In 2021, he completed his PhD studies at the Universidad de Murcia, working on the synthesis and functionality of rotaxanes under the supervision of Professors Jose Berna and Alberto Martinez-Cuezva. The same year, he was awarded with a Margarita Salas postdoctoral contract. His research interests include the synthesis of novel interlocked molecules and their application for the preparation of smart materials.

Aurelia Pastor

Aurelia Pastor graduated in Chemistry and obtained her Ph.D. degree at the Universidad de Murcia. Between 1997 and 1999 she was a Marie Curie postdoctoral fellow at the University of Würzburg (Germany) working with Prof. Waldemar Adam. In 2000 she joined Prof. Mateo Alajarin's Group and one year later she was awarded with a Ramon y Cajal contract. Currently, she is Associate Professor at the Department of Organic Chemistry (Universidad de Murcia). Her research interests include the study of self-assembly processes, the synthesis of interlocked compounds and the application of NMR spectroscopy techniques to the identification of supramolecular structures.

Alberto Martinez-Cuezva

Alberto Martínez-Cuezva graduated in Chemistry at the Universidad de Burgos, where he also received his PhD in 2010. He moved to the Max-Planck Institut für Kohlenforschung (Mülheim an der Ruhr, Germany) as a Postdoctoral Researcher to the group of Prof. Benjamin List (2010-2013). In 2013, he joined the Department of Organic Chemistry at Universidad de Murcia as a Postdoctoral Researcher (Marie-Curie and Juan de la Cierva Fellow). In 2018, he was awarded with a Ramon y Cajal contract and promoted to Assistant Professor. His research interests are focused on the synthesis of novel interlocked compounds, including their employment as advanced organocatalysts in asymmetric transformations.

Guillermo Cutillas-Font

Guillermo Cutillas-Font was born in Cartagena (Spain). He graduated in Chemistry at the Universidad de Murcia in 2019. In 2020 he obtained his Master degree in Fine and Molecular Chemistry at the same University. The same year, he was awarded with a Fundacion Seneca predoctoral contract. He is currently a PhD student within the Synthetic and Organic Chemistry Group of the Universidad de Murcia under the supervision of Professors Aurelia Pastor and Jose Berna. His research interests are focused on supramolecular chemistry, specially synthesis and study of intercomponent and intermolecular interactions in rotaxanes having benyzlic polyamide macrocycles.

Mateo Alajarin

Mateo Alajarin graduated in Chemistry at the Universidad de Murcia, where he also received his PhD. After postdoctoral studies with Prof. Alan R. Katritzky at the University of Florida (United States of America) he returned to the Universidad de Murcia where he is currently Full Professor at its Department of Organic Chemistry. His research interests include novel interlocked compounds, related heterocumulenes, supramolecular chemistry, organophosphorus reagents, tandem processes promoted by H shifts, and other pericyclic and pseudopericyclic reactions.

Jose Berna

Jose Berna graduated in Chemistry at the Universidad de Murcia, where he also received his PhD in 2003. Between 2004 and 2007, he worked as a Postdoctoral Fellow in the group of Prof. David A. Leigh at the University of Edinburgh (United Kingdom). In 2007, he returned to the Department of Organic Chemistry at the Universidad de Murcia as a Postdoctoral Researcher. In 2008, he was awarded with a Ramon y Cajal contract. Currently, he is Associate Professor and his research interests are focussed on the synthesis of novel interlocked compounds oriented towards the development of new functional molecular machines.

Artificial molecular machinery is a research topic with a vast potential either in solution or incorporated into condensed phases. The 2016 Nobel Prize in Chemistry was awarded to Jean-Pierre Sauvage, J. Fraser Stoddart and Bernard L. Feringa, for their contributions to the design of molecular machines.[19–22] Grafting rotaxanes onto the surfaces of materials is a common strategy to build smart materials.[23] In principle, the incorporation of entangled compounds on a condensed solid phase should allow the transfer of the internal dynamics of the MIMs from solution to the solid state, leading to macroscopic applications. In this regard, MOFs have been selected as suitable scaffolds for integrating MIMs in solid-state ordered materials.[24–26] The combination of reticular chemistry[27] and MIMs has resulted in the growth of a new research field giving rise to new materials with interesting properties and applications, by merging the areas of Organic Chemistry, Supramolecular Chemistry, Materials Science and Nanotechnology.

This review is focused exclusively on the use of MIMs as organic linkers in the preparation of the MOFs (or the functionalization of MOF backbones), including the study of their dynamics and applications. Consequently, the polycatenation and polyrotaxanation of the lattice that occurs spontaneously in the formation of several metal-organic structures will not be treated therein.[28–34] For convenience, we have also decided to name the reported reticular materials and the most common ligands as appeared published in their original articles.

2. Mechanically interlocked ligands in metal-organic frameworks

2.1. Rotaxanes as ligands in metal-organic frameworks

Initial strategies for the preparation of Metal-Organic Rotaxane Frameworks (MORFs) relied on the connection of metal ions to the axles of [2]pseudorotaxanes endowed with donor groups (Fig. 2).[35] The use of pseudorotaxanes as building blocks was convenient since they can be easily prepared through a self-assembly driven process, and because once the pseudorotaxanes are bound to the metal nodes the system becomes mechanically locked. In principle, the control over the final structure is imparted by the well-defined geometries of the inorganic joints. Nevertheless, the experimental conditions for the self-assembly and crystallization of the final structure play a crucial role in order to not disrupt the non-covalent interactions during the templated pseudorotaxane formation. Conversely to the use of rotaxanes as building blocks for the synthesis of MOFs, it is possible that some individual components (axles or rings) are incorporated into the crystal lattice when pseudorotaxanes are used as linkers.

This section encompasses from the early materials reported by Kim and designated as rotaxane coordination polymers (RCP) to the most recent and sophisticated MORFs. The roadmap established to have a better control over the spatial arrangement of the mobile components and achieve robust dynamic materials has represented a breakthrough in the synthesis of MIMs-functionalized metal organic frameworks. These guidelines established as key elements the lack of coordination molecules and counterions, a permanently interlocked linker that ensures the retention of the mechanical bond and compact and rigid backbones to minimize skeletal vibrations in the resulting framework.[25,26,36,37]

2.1.1. [2]Pseudorotaxane linkers with cucurbit[n]urils

Kim was the first synthesizing 1D, 2D or 3D polyrotaxanes with high structural regularities in solid state.[38] Kim's strategy was based on the high affinity of cucurbit[6]uril (**CB[6]**) toward alkyl diammonium ions to form stable pseudorotaxanes, which were then connected with transition metal nodes (Fig. 3).

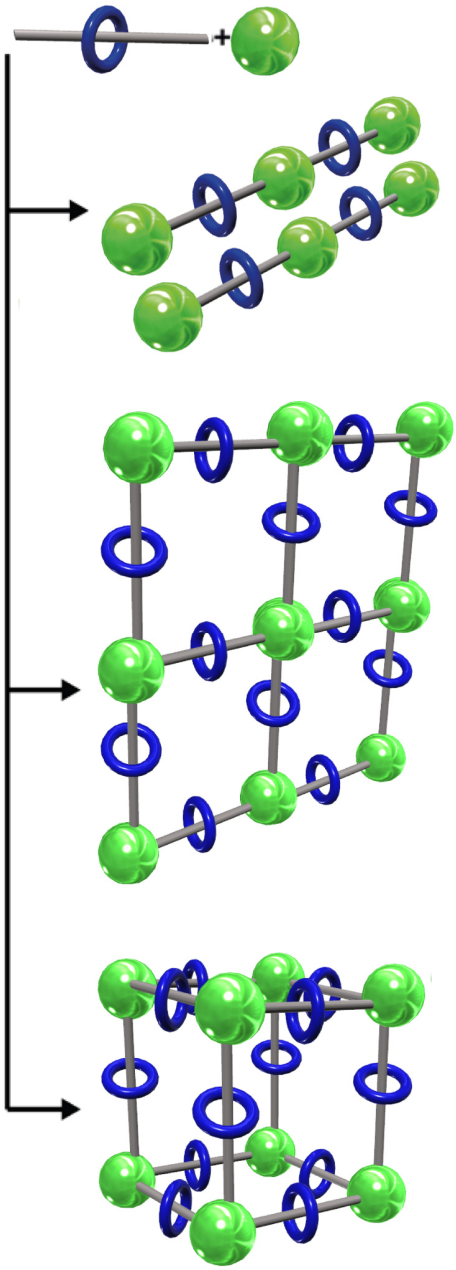

Fig. 2 Cartoons showing one-, two- and three-periodic coordination polymers built from [2]pseudorotaxane linkers and metal joints.

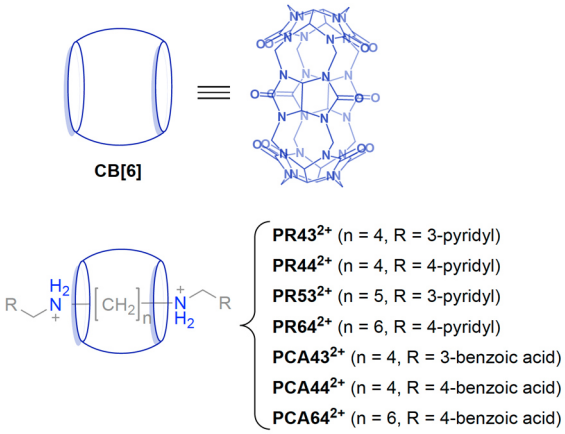

Fig. 3 [2]Pseudorotaxanes formed by the inclusion of protonated diaminoalkane axles into **CB[6]**.[38]

One-periodic coordination polymers were obtained from pseudorotaxanes **PR43²⁺**, **PR44²⁺** or **PR53²⁺** and Ag(I), Cu(II), Ni(II), Co(II) or Cd(II) nitrate salts under hydrothermal conditions.[38,39,40] The nature of the metal node determines the zigzag, square-wave or helical structure of the 1D framework. Thus, the reaction of $Cu(NO_3)_2$ with **PR44²⁺** led to the zigzag one-periodic coordination polymer **MORF-1** (Fig. 4a).

Counter-anions also play a key role, thus when silver tosylate was treated with ligand **PR44²⁺** a 1D polyrotaxane was formed. However, the change to silver nitrate led to a novel two-periodic hexagonal net with a silver ion at each corner and a pseudorotaxane at the edges (**MORF-2**, Fig. 4b).[41] This network is perpendicularly interpenetrated with another one, resulting in the first example of a polycatenated 2D polyrotaxane structure. By contrast, the combination of silver triflate or copper(II) nitrate and **PR43²⁺** ligands having 3-pyridyl groups at the terminals, led to a two-periodic coordination polymer containing square grids between rotaxane subunits.[40]

In 2000, Kim and co-workers reported the first three periodic rotaxane coordination polymer $[Tb_2(H_2O)_4(\mathbf{PCA43})_3][\mathbf{H_2PCA43}][NO_3]_4[OH]_4{\cdot}40H_2O$ (**MORF-3**), prepared under hydrothermal conditions.[42] The presence of the lanthanide metal ion, with a larger ionic radius and a higher coordination number, is crucial for the formation of the 3D framework. The basic building unit of **MORF-3** consists of a binuclear Tb(III) cluster behaving as a six-connected node for the carboxylate groups of the ligand **PCA43²⁺**. The 3D polyrotaxane network features a non-interpenetrated inclined α-polonium topology (Fig. 4c).

Su and co-workers drew on dynamic combinatorial coordination chemistry to prepare a novel MORF with formula $[Cu(\mathbf{PCA64})(\mathbf{PCA64}^{2-})]{\cdot}13H_2O$.[43] Through pH-changes they introduced flexibility into the thread leading to a unique combinatorial fashion of *trans*/*cis*-rotaxanes. The 1D zigzag polyrotaxane chains of *cis* ligands extend to a wavy hexagonal subnet through the connection of *trans* rotaxanes. The interpenetration of different layers leads to a 3D self-catenated network.

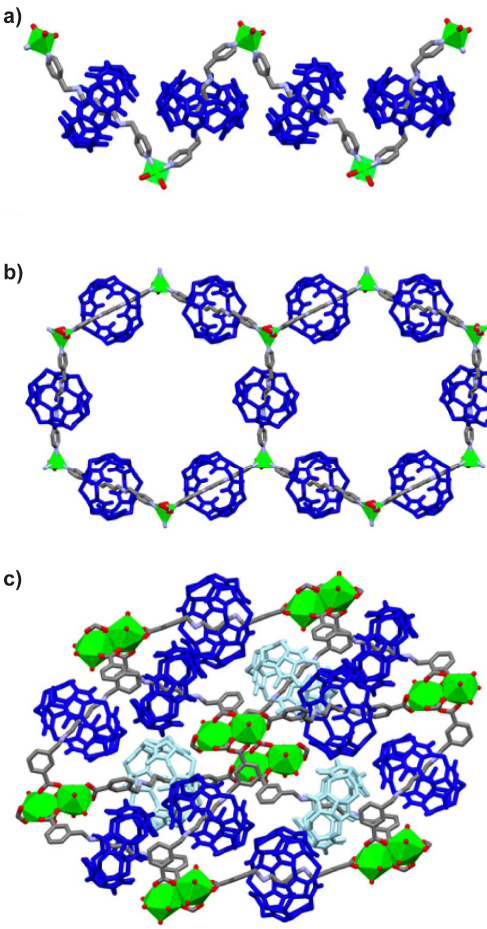

Fig. 4 (a) Linear one-periodic coordination polymer **MORF-1** consisting of Cu(II) nodes and **PR44²⁺** linkers;[39] (b) two-periodic coordination polymer **MORF-2** formed by Ag(I) nodes and **PR44²⁺** linkers resulting in a hexagonal net;[41] and (c) α-polonium-like net showed by **MORF-3** featuring binuclear Tb(III) clusters and **PCA43²⁺** linkers.[42] Hydrogen atoms and interpenetration are omitted for clarity. Colour key: dark and light blue = **CB[6]**; grey = carbon atoms; blue = nitrogen atoms; red = oxygen atoms; and green = copper, silver or terbium atoms.

The use of mixed ligands for fabricating MORFs constitutes a powerful strategy to increase the diversity of structures and functions. Furthermore, the coordination sphere of the metal cluster can be tuned by changing the temperature, geometry and length of the auxiliary ligand in order to obtain high-dimensional MORFs. Su and co-workers employed this methodology to prepare a set of novel MORFs from the pseudorotaxane **PR43²⁺**, rigid carboxylate ligands derived from terephthalic acid (**H_2BDC**) and cadmium ions (Fig. 5a).[44] Thus, **MORF-4** of formula $Cd_4[\mathbf{PR43}]_2[\mathbf{BDC}]_2Cl_4{\cdot}7H_2O$ was formed under hydrothermal conditions at 100 °C. **MORF-4** is built by binuclear cadmium clusters linked by **BDC²⁻** ligands forming infinite chains. These chains are interconnected by pseudorotaxane linkers to furnish a 3D MORF featuring spacious diamondoid cages able to interpenetrate (schematically represented in Fig. 5b). The authors also observed that an increase in the temperature influences on the

degree of interpenetration and symmetry of the MORF structure.[44] Thus, if the self-assembly of the components takes places at 120 °C a new MORF, Cd_2[**PR43**][**BDC**]$_2Cl_2 \cdot 8H_2O$ (**MORF-5**) is formed, where two periodic layers are built by binuclear cadmium clusters and $\mathbf{BDC}^{2-}$ ligands. These two-dimensional layers are further linked by $\mathbf{PR43}^{2+}$ pseudorotaxanes pillars to form a 3D MORF of *pcu* topology (schematically represented in Fig. 5c). There is no interpenetration in **MORF-5** due to the small pores along its reticular network.

Su and co-workers also extended the mixed-ligand strategy to the preparation of 3D MORFs with diverse rigid carboxylate ligands and d^{10} metal ions, demonstrating that non-covalent interactions around **CB[6]**, such as hydrogen bonding, C-H···π and π···π interactions, could affect the formation of the resulting solid hybrids.[45] In 2018, again the group of Su prepared the first 3D porous **CB[6]**-based MORF $[Cu_2(\mathbf{PR44})_{0.5}(\mathbf{BDC})_2Cl] \cdot 3DMF$ (**MORF-6**) synthesized under solvothermal conditions.[46]

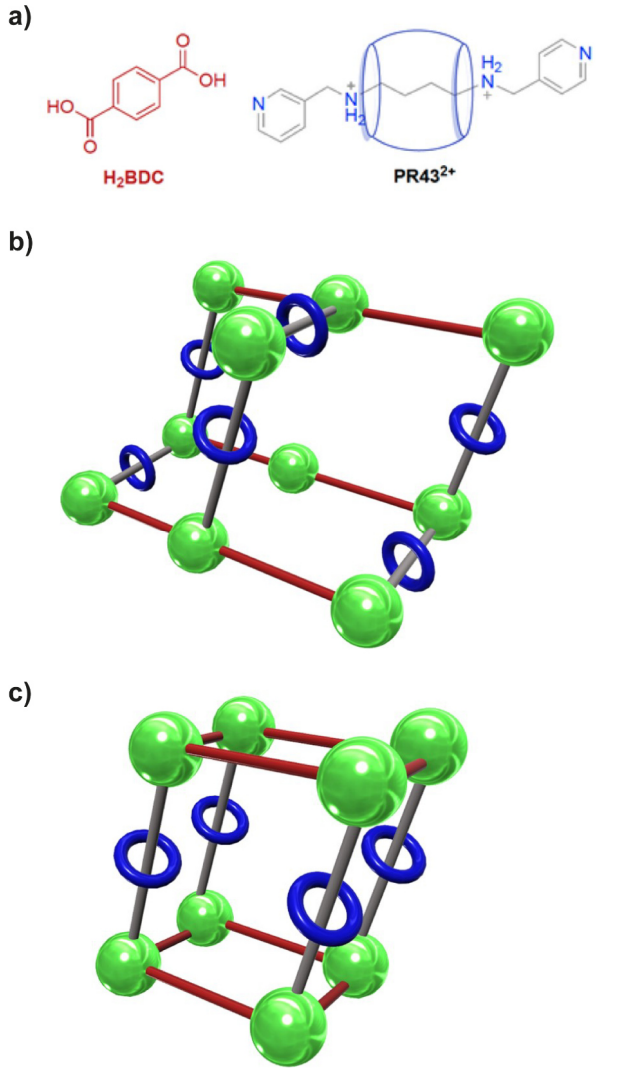

Fig. 5 (a) Chemical structure of the organic struts used as building blocks of **MORF-4** and **MORF-5**; (b) schematic view of a single diamondoid cage of **MORF-4**; and (c) schematic illustration of a *pcu* unit in **MORF-5**.[44]

Through an ion exchange reaction, the nitrate group of the starting $[\mathbf{PR44}]^{2+} \cdot 2[NO_3]^-$ was replaced by an hexafluorophosphate ion which turned out soluble in DMF. The structure of **MORF-6** showed a 3D pillared-layer structure in which 2D sheets of $[Cu_2\mathbf{BDC}_2Cl]$ are connected by $\mathbf{PR44}^{2+}$ pseudorotaxanes (Fig. 6).

MORF-6 forms hexagonal open channels along the crystallographic *c* axis with a potential solvent accessible area close to 46% of the crystal volume. Solvent-exchange has been investigated by different techniques. Recently, the same research group have synthesized new **CB[6]**-based pseudorotaxanes MORFs containing Co(II)[47] or Cu(II)[48] ions which show interesting properties such as antiferromagnetic exchange interactions or high proton conductivity.

Additionally, MORFs containing **CB[n]s** other than **CB[6]** have been reported. Thus, Kermagoret, Bardelang and co-workers have described a Zn-based 3D-MORF built from rigid pillars derived from **CB[7]** units threaded by a viologen axle.[49] The colour of the resulting 3D-MORF crystals reversible changes from pale yellow to green when exposed to UV light. The photochromism featured by these crystals is presumably due to the electron transfer from the carboxylic acid functions to the viologen moiety favoured by the short distances in the MOF structure.[50] This interesting property could find applications in inkless printing or transient writing/erasing for data encryption.

Recently, Sun and co-workers have prepared the first MORF with a negatively-charged tricarboxylate ligand encapsulated into the cavity of a **CB[7]**-based pseudorotaxane.[51] This porous Sr-based 3D MORF, obtained under hydrothermal conditions, effectively absorbs iodine and selectively capture K^+ among a mixture of other alkali metal ions.

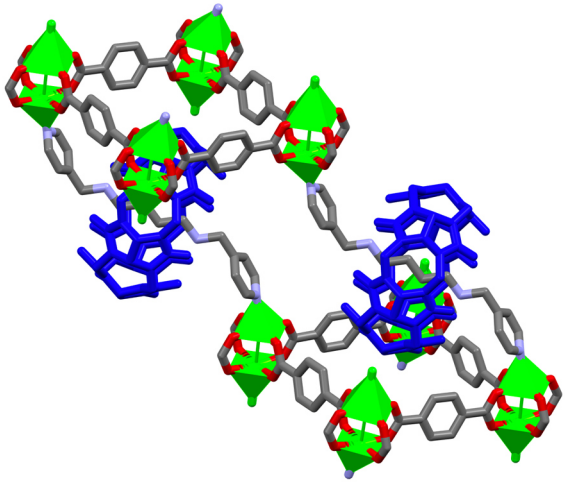

Fig. 6 Illustration of the cavity of **MORF-6** formed by 2D sheets of $[Cu_2\mathbf{BDC}_2Cl]$ connected by $\mathbf{PR44}^{2+}$ linkers. Hydrogen atoms are omitted for clarity in the solid structure. Colour key: dark blue = CB[6]; grey = carbon atoms; blue = nitrogen atoms; red = oxygen atoms; and green = chlorine and copper atoms.[46]

2.1.2. [2]Pseudorotaxane linkers with pyridinium axles and crown ether wheels

In 1998 Loeb and co-workers reported a new type of [2]pseudorotaxanes formed by the efficient assembly of 1,2-bis(pyridinium)ethane dication axles and [24]crown-8 ether wheels through a combination of hydrogen bonding, ion-dipole and π-stacking interactions (Fig. 7, X = N and R^1/R^2 = H).[52,53] The connection of these new interlocked linkers through transition metal ions led to a new set of coordination polyrotaxanes and MORFs. The advantages of this new approach includes the fine control of the internal properties of these materials (i.e. pore size, hydrophobicity of the framework) just by replacing the crown ether structure.[54]

The one-periodic **MORF-7** of formula $[Co(H_2O)_2(MeCN)_2(\mathbf{1}\subset\mathbf{DB24C8})][BF_4]_4\cdot(MeCN)_2(H_2O)_2$ formed from 1,2-bis(pyridinium)ethane dication $\mathbf{1}^{2+}$ in the presence of benzo[24]crown-6 and Co(II) metal ions (Fig. 8a).[55] The *anti* conformation at the central ethylene unit of the axle and the *trans* geometry at the octahedral metal ion are key structural features governing the linearity of this coordination polymer.

The 2D network (**MORF-8**), having an overall formula $[Cd(H_2O)(BF_4)(\mathbf{1}\subset\mathbf{DB24C8})_2]\cdot[BF_4]_5\cdot(MeNO_2)_{15}$, was obtained in the presence of a noncoordinating solvent such as nitromethane, by using a greater amount of [2]pseudorotaxane and Cd(II) as metal node (Fig. 8b).[55] Every Cd(II) metal ion has an octahedral geometry and is connected to four pyridyl groups of the rotaxane linkers leading to a square planar arrangement. A water molecule and a BF_4^- anion complete the metal coordination sphere. The resulting 2D MORF forms square nets and possesses larger cavities with no interpenetration, which ultimately lead to the presence of channels along the *c* axis. Probably, the 3D network did not form due to steric crowding around the metal ion.

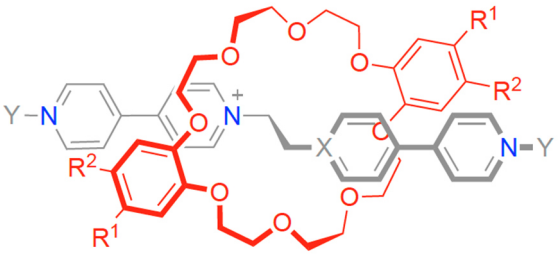

$[\mathbf{1}\subset\mathbf{DB24C8}]^{2+}$ X = N R^1/R^2 = H

$[\mathbf{1}\subset\mathbf{TPDB24C8}]^{2+}$ X = N $R^1/R^2 = CH_2OPh$

$[\mathbf{2}\subset\mathbf{DB24C8}]^{2+}$ X = N R^1/R^2 = H Y = O

$[\mathbf{1}\subset\mathbf{DSDB24C8}]$ X = N $R^1 = SO_3^-$, R^2 = H

$[\mathbf{3}\subset\mathbf{DSDB24C8}]^-$ X = C $R^1 = SO_3^-$, R^2 = H

Fig. 7 [2]pseudorotaxanes designed by Loeb and co-workers formed by pyridinium axles and crown ether wheels.[56]

In order to prove the tunability of this methodology, four phenoxy groups were incorporated into the macrocycle. Thus, a new MORF was prepared from $[\mathbf{1}\subset\mathbf{TPDB24C8}]^{2+}$ and a Cd(II) salt. Despite this material is a two-periodic coordination polymer, the larger size of the macrocycle lead to a one dimension array of interlocked linkers pillared by naked axles.[57] An analogous pattern was observed with the bis *N*-oxide $[\mathbf{2}\subset\mathbf{DB24C8}]^{2+}$ struts, although in this case the alternating layers of square grids are filled by crown ether units of neighbouring sheets, thus avoiding the formation of infinite channels.[58]

The use of lanthanide ions as metal nodes turned out to be a pivotal factor for increasing the order of dimensionality of the resulting MORF. Thus, Loeb and co-workers could prepare the set of materials **MORF-9** from the reaction of $\mathbf{[2\subset DB24C8][OTf]_2}$ with different $M(OTf)_3$ (M = Sm, Eu, Gd or Tb) in acetonitrile.[59] In this case, the metal centre features an square antiprismatic eight-coordinate geometry involving six pyridine *N*-oxide rotaxanes as linkers, one water molecule and one triflate anion. The 3D metal-organic framework comprises an α-polonium net with only a single interpenetration.

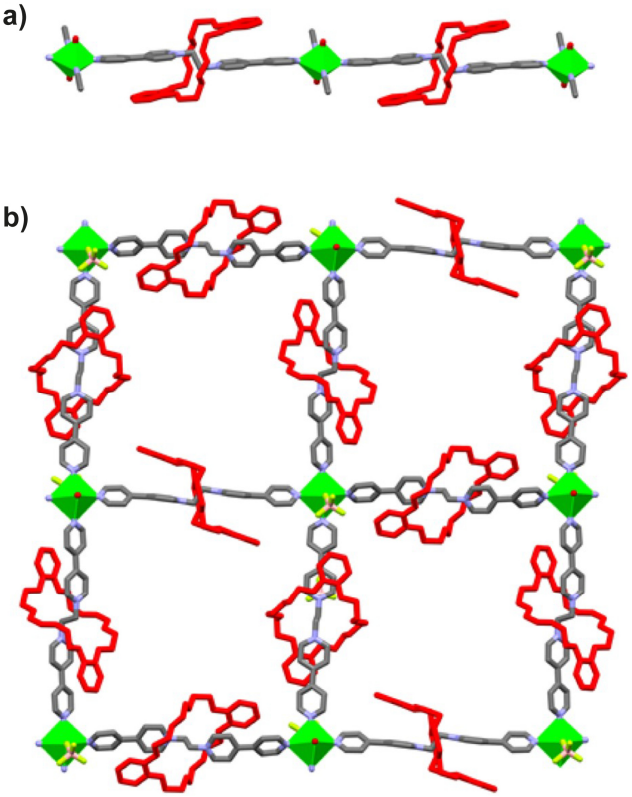

Fig. 8 (a) Linear one-periodic coordination polymer **MORF-7** formed by Co(II) nodes and $[\mathbf{1}\subset\mathbf{DB24C8}]^{2+}$ linkers; and (b) two-periodic coordination polymer **MORF-8** with Cd(II) nodes and $[\mathbf{1}\subset\mathbf{DB24C8}]^{2+}$ linkers.[55] Hydrogen atoms are omitted for clarity. Colour key: red = **DB24C8** and oxygen atoms; grey = carbon atoms; blue = nitrogen atoms; yellow = fluorine atoms and green = cobalt and cadmium atoms.

Curiously, the change to a smaller-radius metal Yb(III) results in a completely different material (**MORF-10**) of formula [Yb(OTf)(**2⊂DB24C8**)$_3$][Cl][OTf]$_7$. In **MORF-10** the metal ion adopts a pentagonal bipyramidal geometry with five-coordinated *N*-oxide rotaxanes held in equatorial plane, one additional rotaxane and a triflate ion placed at the axial positions. The five rotaxanes at the equatorial positions arrange in a peculiar net of alternating triangles and squares connected through the metallic nodes (schematically represented in Fig. 9). The large square cavities allow interpenetration. Notably, TGA analyses of **MORF-9** and **MORF-10** showed stable phases until 240 °C.[59]

In the search of a robust and truly porous MORF that could allow the dynamic behaviour of the wheel, Loeb and co-workers designed a neutral framework to overcome the need for space-filling counterions. Thus, the treatment of a disulfonated dibenzo-24-crown-8 ether wheel **DSDB24C8**$^{2-}$ and a dicationic 1,2-bis(pyridinium)ethane axle **1**$^{2+}$ yielded a neutral [2]pseudorotaxane (Fig. 7) which in combination with a neutral metallic node, such as a $Cu_2(BzO)_4$ paddlewheel, led to the linear one-dimensional **MORF-11** of formula [$Cu_2(BzO)_4$(**1⊂DSDB24C8**)](MeOH)$_2$(DMF) (Fig. 10).[60] In this material, two Cu(II) metals with square pyramidal geometry form a binuclear cluster. Four benzoate groups join the two copper ions at the equatorial sites whereas at the axial sites coordinated the neutral linkers. The linear strands are organized in a parallel fashion. The lack of counterions results in a very efficient packing filled with only two molecules of MeOH and one of DMF per asymmetric unit.

In a further stage, Loeb and co-workers prepared **MORF-12** and **MORF-13** by combination of the cyclochiral pseudorotaxane **[3⊂DSDB24C8]**$^-$, prepared by self-assembly of the monocationic pyridinium axle **3**$^+$ and **DSDB24C8**$^{2-}$ (Fig. 7), with Zn(II) ions.[61] In the presence of equimolecular amounts of pseudorotaxane linker and metal ion, a one-periodic **MORF-12** of formula [Zn(**3⊂DSDB24C8**)(H_2O)$_2$(MeOH)][NO_3]·2MeOH is obtained, where two bridging ligands of the same chirality coordinate in a *trans* arrangement to an octahedral Zn(II) (Fig. 11a).

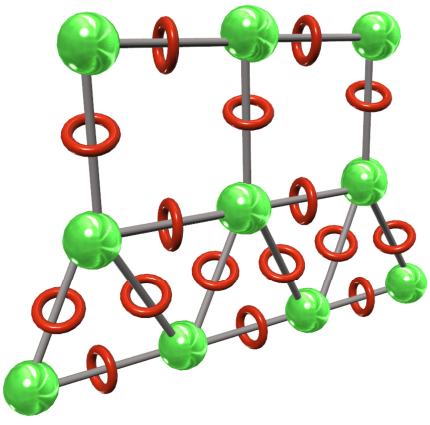

Fig. 9 Cartoon representing the two-dimensional layers of the three-periodic **MORF-10** consisting of alternating square and triangular forms.[59]

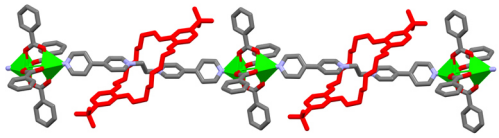

Fig. 10 Linear strand of the charge neutral 1D **MORF-11** consisting of $Cu_2(BzO)_4$ paddlewheel nodes and [**1⊂DSDB24C8**] linkers.[60] Hydrogen atoms are omitted for clarity. Colour key: red = **DSDB24C8**$^{2-}$ and oxygen atoms; grey = carbon atoms; blue = nitrogen atoms; and green = copper atoms.

Interestingly, two strands of opposite chirality are joined in a head-to-tail fashion by coordination of a sulfonate group to a Zn(II) metal ion of a neighbouring strand.[61] The remaining coordinating positions are filled by water and methanol molecules.

When the amount of linker double that of the metal ion, the neutral and two-periodic **MORF-13** of formula [Zn(**3⊂DSDB24C8**)$_2$(H_2O)$_2$]·H_2O·21$MeNO_2$, was formed (Fig. 11b).[61] In this case, four pyridine groups are coordinated to the equatorial sites of the Zn(II) cations, while molecules of water occupied the remaining sites to give an enantiomerically pure square grid. The two-dimensional layers stack in an alternating fashion through hydrogen bonding between the axially coordinated water molecules to give a racemic framework. Immersion of **MORF-13** in chloroform and further drying under mild vacuum at room temperature gave a solvent-free porous solid. Interestingly, when the same components are combined in the presence of sulphate anions a three-periodic coordination polymer is built. In this case, the neutral square grids are pillared by [Zn(MeOH)$_2$(H_2O)$_2$(SO_4)$_2$]-based clusters giving a 3D coordination polymer with a higher stability.[61]

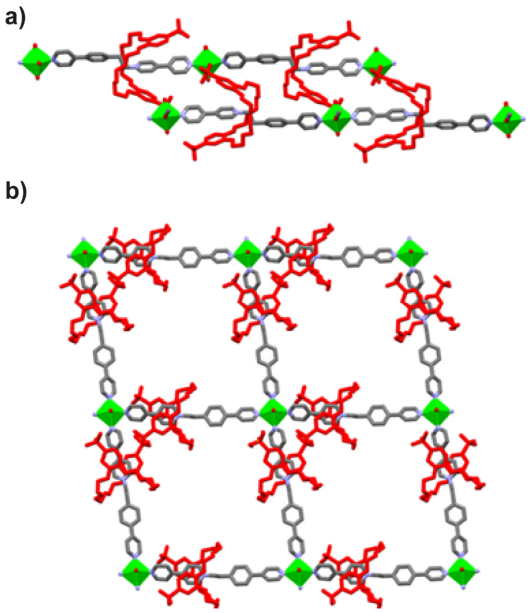

Fig. 11 (a) Two antiparallel strands of the 1D **MORF-12** consisting of Zn(II) nodes and [**3⊂DSDB24C8**] linkers; and (b) square grid of neutral 2D **MORF-13** formed by Zn(II) nodes and [**3⊂DSDB24C8**] linkers. Hydrogen atoms are omitted for clarity.[61] Colour key: red = **DSDB24C8**$^{2-}$ and oxygen atoms; grey = carbon atoms; blue = nitrogen atoms; and green = zinc atoms.

2.1.3. [2]Rotaxane linkers with coordinating groups in the wheel

In 2011 Loeb and co-workers envisioned a completely different approach that switches the roles of axle and wheel, with the ring acting as linker that connects the metal nodes.[62] First, the precursor [2]rotaxane **4**$^{2+}$ bearing nitrogen donor groups at the 4- and 5-positions of the crown ether aromatic rings was synthesized and used as ligand to coordinate Cd(II) ions (Fig. 12a). The resulting two-periodic framework **MORF-14** has the binuclear cluster $[(H_2O)_2Cd(\mu\text{-}Cl)_2Cd(H_2O)_2]$ as node to which four pyridyl groups of a single macrocycle coordinate to the axial sites of four different metal nodes (Fig. 12b). The resulting material features large clefts, the wheels, through which the axles are threaded.

In a more recent example, Berna and co-workers described photoresponsive MORFs using benzylic amide [2]rotaxanes as organic linkers and Cu(II) ions as metal nodes (see Section 4, focused on stimuli-responsive MORFs, for a more detailed description).[63]

2.1.4. [2]Rotaxane linkers with coordinating groups in the axle and the wheel

The multidentate [2]rotaxane ligand **5**$^{2+}$ contains four thioether functions appended to the crown ether and two more at the terminals of the linear axle (Fig. 13a).[64] When this ligand reacted with AgOTf a new material of formula $[Ag_6(\mathbf{5})_2(OTf)_6(MeCN)_2(MeOH)_2][OTf]_4(MeCN)_4$ (**MORF-15**) was formed.

In this network there are two metal nodes composed of binuclear Ag centres with pseudotetrahedral geometry and the six thioether sulphur atoms are bonded to at least one Ag metal ion. The resulting framework incorporates two types of interpenetration due to both the interlocked structure of the ligands and that inherent to the lattice, which adds a higher level of complexity to these systems. Notably, even though the basic network consists of these complex interwoven strands, there is still large openings of void space (Fig. 13b).

Loeb and co-workers synthesized two more examples of polythreaded MORFs based on a rigid H-shaped axle containing two benzimidazole recognition sites and a crown ether-based macrocycle (see Section 4 for a more detailed description of this kind of systems). First, an hexadentate ligand was synthesized containing four carboxylate groups at the H-shaped thread and two other carboxylate moieties to the crown ether.[65] The resulting MORF was obtained by reaction with zinc nitrate under solvothermal conditions. The network is characterized by three interpenetrated lattices each one built of alternating threads and macrocycles. The origin of the interpenetration is the interlocked nature of both linkers, the thread and the wheel. Alternatively, Cu(II) and Zn(II) MORFs were prepared from a tetracarboxylate H-shaped axle and a macrocycle bearing two 4-pyridyl groups.[66]

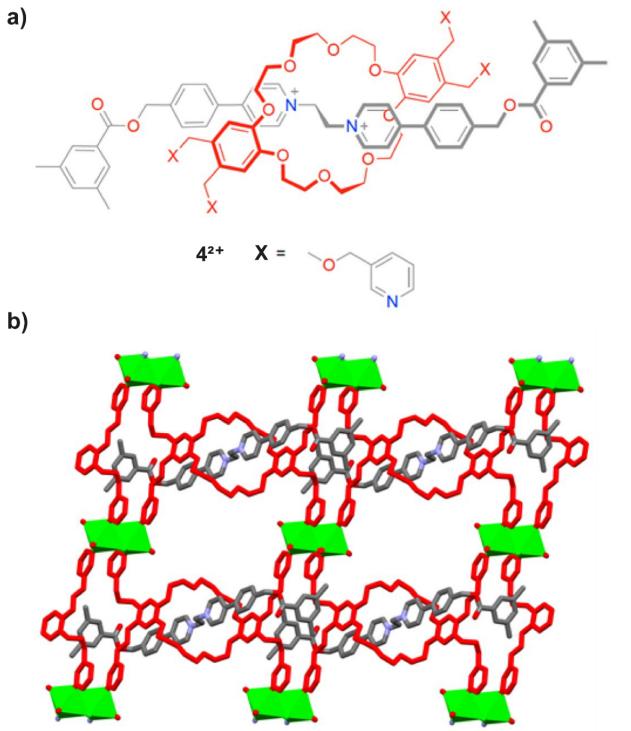

Fig. 12 (a) Structure of the rotaxane **4**$^{2+}$ used as a linker in **MORF-14**; and (b) the two-periodic coordination polymer **MORF-14** consisting of $[(H_2O)_2Cd(\mu\text{-}Cl)_2Cd(H_2O)_2]$ nodes and **4**$^{2+}$ rotaxane linkers.[62] Hydrogen atoms are omitted for clarity in the solid structure. Colour key: red = Macrocycle and oxygen atoms; grey = carbon atoms; blue = nitrogen atoms; and green = chlorine and cadmium atoms.

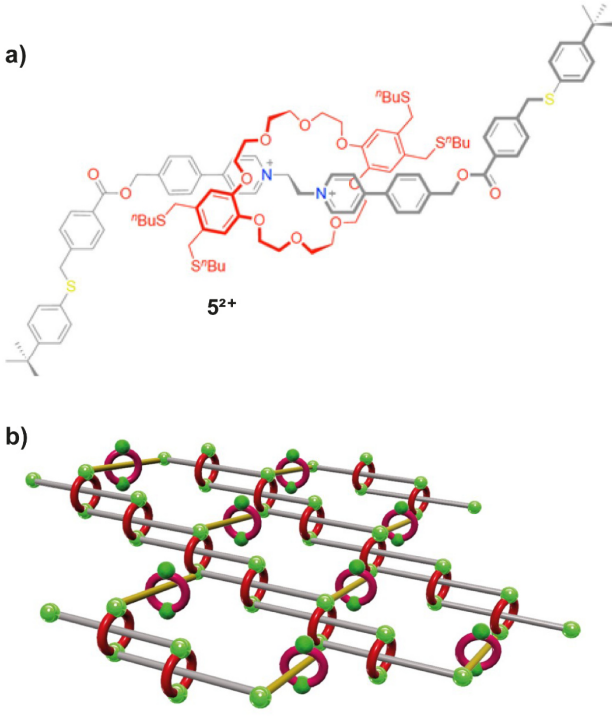

Fig. 13 (a) Structure of the rotaxane **5**$^{2+}$ used as linker in the knitted **MORF-15**; and (b) a cartoon depicting the network and how various strands intertwine in the lattice of **MORF-15.**[64]

2.1.5. [2]Pseudorotaxane linkers with a Texas-sized molecular box

Sessler and co-workers developed a facile one-step, self-assembly approach to the construction of MORFs employing the [2]pseudorotaxane $\mathbf{6}^{2+}$ comprised of the imidazolium-based macrocycle, named by the author as Texas-Sized Molecular Box (**TSMB**$^{4+}$), and the 2,6-naphthalene dicarboxylate axle (**NDC**$^{2-}$) as axle (Fig. 14a).[67] A typical feature of **TSMB**$^{4+}$ is its conformational flexibility and so its ability to change its shape in order to accommodate guests of different size and shape. The combination of **TSMB**$^{4+}$, **H_2NDC** and a Zn(II) salt in the presence of triethylamine led to **MORF-16**, which constitutes the first example of an anion-complexation-directed assembly of a mechanically linked MORF (Fig. 14b).

MORF-16 is a highly ordered, interlocked 3D structure composed of [**TSMB**·(**NDC**)$_4$·Zn_2]·6H_2O subunits. In **MORF-16**, each metal centre is coordinated to four carboxylate groups in a tetrahedral geometry to form an interpenetrated twisted adamantane-like network in which one out of each four linkers is encircled by a **TSMB**$^{4+}$ macrocycle (Fig. 14b). The system is stabilized by cation complexation and donor-acceptor interactions. Voids in the structure are filled by interpenetration of another framework and water molecules. Despite its low porosity, the material shows multilayer adsorption behaviour. Thermogravimetric analysis and PXRD measurements showed **MORF-16** to be thermally stable up to 230 °C.

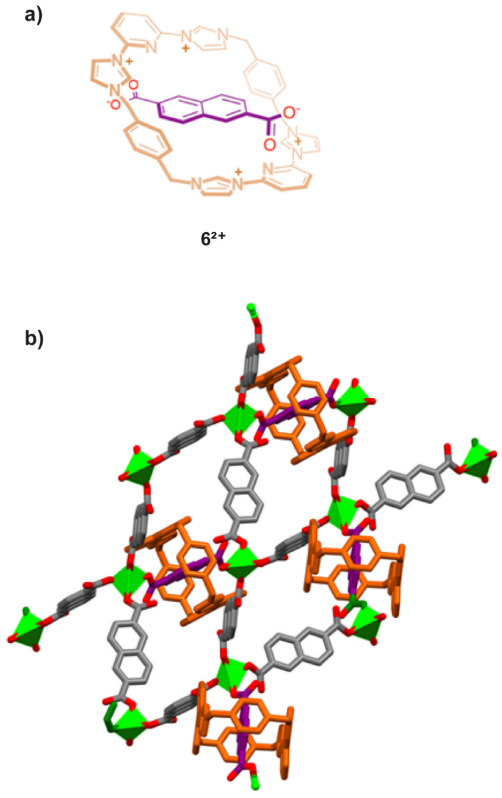

Fig. 14 (a) Chemical structure of [2]pseudorotaxane $\mathbf{6}^{2+}$; and (b) X-ray structure of the twisted tetrahedron subunit **[TSMB·(NDC)$_4$·Zn$_2$]** in **MORF-16**.[67] Hydrogen atoms and interpenetration are omitted for clarity. Colour key: Burnt orange = **TSMB**$^{4+}$; grey = carbon atoms; red = oxygen atoms; and green = zinc atoms. Axles encircled by the wheel have been coloured in purple.

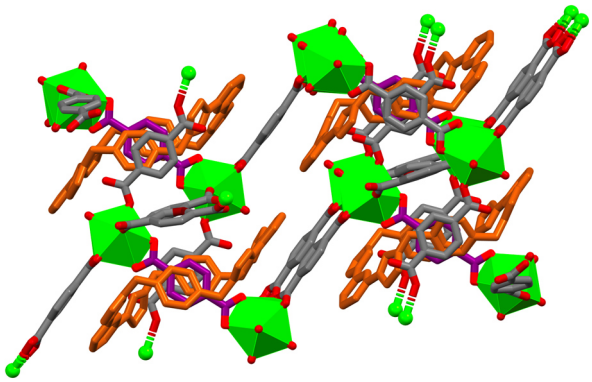

Fig. 15 X-ray structure of **MORF-Eu**.[68] Hydrogen atoms are omitted for clarity. Colour key: Burnt orange = **TSMB**$^{4+}$; grey = carbon atoms; red = oxygen atoms; and green = europium atoms. Axles encircled by the wheel have been coloured in purple.

Sessler and co-workers also described the first luminescent MORFs built from **TSMB**$^{4+}$, the terephthalate dianion (**BDC**$^{2-}$) and lanthanide metal cations such as Nd(III), Sm(III), Eu(III) and Tb(III).[68] In the **MORF-Eu** of formula [**TSMB**(**BDC**)$_5$$Eu_2$($H_2O$)$_3$]·16$H_2O$, the lanthanide adopts two different coordination modes involving the oxygen atoms of the dianion and coordinated water molecules (Fig. 15). The macrocycles **TSMB**$^{4+}$ are threaded by **BDC**$^{2-}$ in a single direction. These authors demonstrated that the nature of the lanthanide cation has a strong influence on the structural and optical properties of the material, which could afford a procedure to discern between this series of lanthanide cations.

In a further seminal study, Sessler and co-workers showed that the incorporation of substituents at the terephthalate dianion plays a critical role in modulating both the self-assembly with **TSMB**$^{4+}$ and the coordination with a given metal cation to produce different types of MOFs, SOFs, RSOFs or MORFs.[69]

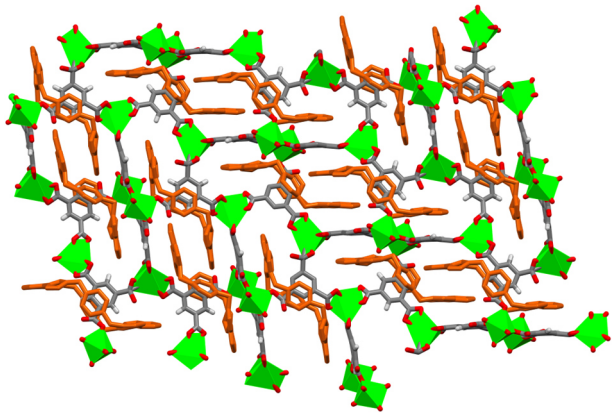

Fig. 16 X-ray structure of the 2D-periodic **MORF-17**.[70] Hydrogen atoms are omitted for clarity. Colour key: Burnt orange = **TSMB**$^{4+}$; grey = carbon atoms; red = oxygen atoms; and green = cadmium atoms.

A 2D-periodic **MORF-17** can be also prepared by direct self-assembly of **TSMB^{4+}**, benzene-1,3,5,-tricarboxylate (**BTC^{3-}**) and Cd(II) ions.[70] The X-ray structure of **MORF-17**, with formula [**TSMB**$_2$·(**BTC**)$_4$·Cd$_4$·(OH)$_4$·4H$_2$O,]·19H$_2$O, showed that **TSMB^{4+}** macrocycles surround the edge of the anionic **BTC^{3-}** subunits while Cd(II) cations are acting as nodes (Fig. 16).

Recently, Gong and co-workers described a set of MORFs (**MORF-Pb-1** and **MORF-Pb-2**) constructed from **TSMB^{4+}**, **BDC^{2-}** and **NDC^{2-}** dianions and Pb(II) cation.[71] Unusual Pb···Pb weak interactions were found in the former.

2.1.6. Post-synthetic strategy for the generation of MORFs with active domains.

Yaghi, Stoddart and co-workers were able to incorporate molecular recognition sites in MOFs (active domains) into which incoming guests can dock by means of stereoelectronic control.[72] In this sense, the linear ligand **7** containing an electron-rich macrocycle, which is known to act as receptor for electron-deficient guests such as the paraquat dication (**PQT^{2+}**) (Fig. 17a), was used as linker to prepare **MOF-1001** in combination with Zn(II) salts.

MOF-1001 presents a cubic non-interpenetrated lattice where eight [Zn$_4$O(CO$_2$)$_6$] polyhedra are placed at the corners while twelve macrocycles are held at the edges of the cubic net, schematically represented in Fig. 17b. In a post-synthetic strategy, **MOF-1001** was exposed to a saturated solution of **PQT^{2+}** in acetone. The crystals of **MOF-1001** turned from yellow to red due to the threading of the guests through the crown ethers and the formation of donor-aceptor [2]rotaxanes (Fig. 17b). The paraquat dication can be easily removed from **MOF-1001** upon rinsing with acetone.

A homochiral version of **MOF-1001** was also prepared by using a solvothermal procedure wherein a DMF solution of an axially-chiral crown ether-containing struts was heated for a 24 h period in the presence of Zn(II) ions. The single-crystal X-ray of the resulting framework, **(*SS*)-MOF-1020**, revealed a structure isoreticular with **MOF-1001**.[73]

P5A-MOF-1, with A1/A2-difunctionalized pillar[5]arene struts and Zn$_4$O secondary building units,[74] has also an active domain that selective uptakes neutral and positively charged electron-poor aromatic guests such as the *N*,*N*'-dihexyl-4,4'-bipyridinium dications due to charge transfer interactions.

Some advances in reticular chemistry demonstrated that SALI (Solvent-Assisted Ligand Incorporation) technique is useful for the preparation of new MOFs unavailable by other synthetic methods.[75,76] In 2015, Stoddart and co-workers used the SALI strategy for the inclusion of MIMs within the pores of a prefabricated MOF.[77] In this strategy, rigid triradical semirotaxanes, which are first formed in solution, diffuse through the channels of the MOF (**NU-1000**) and attached to the coordination sites (Zr-clusters) through its non-stoppered end (see Figure 32 and Section 4.1 for a more extended description of this system).

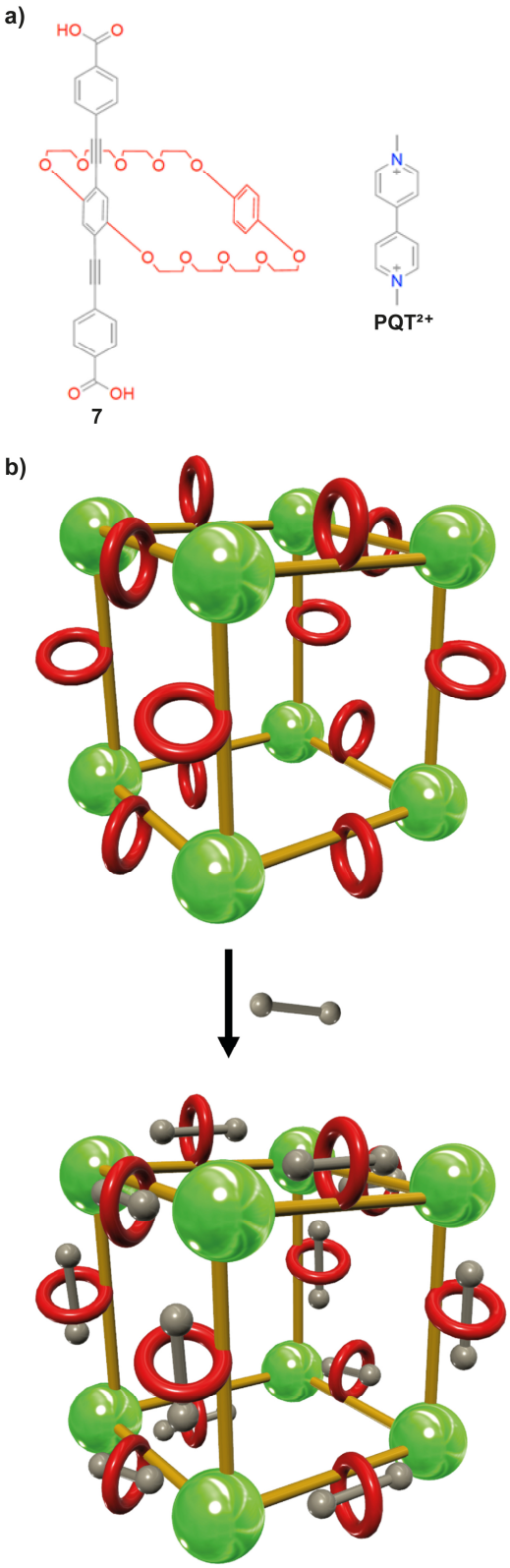

Fig. 17 (a) Structure of linker **7** and **PQT^{2+}**; and (b) cartoon representing the docking of **PQT^{2+}** into the recognition sites of **MOF-1001**.[72]

Due to their structural and chemical diversity and good biocompatibility, MOFs have brought the attention of the scientific community as potential candidates for the next generation of cancer theranostic agents. Yang and co-workers

have reported the preparation of a MOF core-shell hybrid endowed with pillararene-based pseudorotaxanes on the surface.[78] This new material is able to act as a biocompatible nanovalve for on-command drug release in MRI-guided cancer therapy, in response to pH changes, temperature variations and competitive agents.

2.1.7. A linker containing a Cu(I) templated [2]pseudorotaxane

Metal-containing MIMs offer the opportunity to introduce switches within MOFs. Stoddart, Sauvage, Yaghi and co-workers successfully incorporated the switchable [2]pseudorotaxane based linker **[8·Cu]⁺** in a MORF (Fig. 18).[79] The combination of **[8·Cu]⁺** with Zn(II) ions under solvothermal conditions resulted in **MOF-1040** as red cubic crystals. **MOF-1040** presents a threefold interpenetrated network with a *pcu* topology where Zn_4O units act as nodes linked by rotaxanate-based struts **[8·Cu]⁺**. Treatment of **MOF-1040** with oxone produces local electronic switches originated by the partial oxidation of Cu(I) to Cu(II) ion centres, as shown by EPR experiments. Furthermore, partial demetalation of the rotaxane linkers in **MOF-1040** was conducted by treatment with KCN. PXRD patterns of the material demonstrate that the structural topology is retained after oxidation or demetalation.

2.1.8. MORFs based on [3]rotaxanes and nanotubes

Winpenny and co-workers synthesized a new type of 1D MORF based on the [3]rotaxane **9** formed by two {Cr_7Ni} clusters surrounding a *N*,*N*′-bis(pyridin-4-ylmethyl)decane-1,10-diamonium thread (Fig. 19).[80] The two pyridyl groups at the ends of the thread coordinate to $[Cu_2(O_2C^tBu)_4]$ units in the final material.

Lu and co-workers prepared an unprecedented 3D dynamic MORF.[81] In this framework, four **[NiL]²⁺** (Fig. 20) are connected by four **TCBA³⁻** (tri(4-carboxybenzyl)amine) anions to build a tetragonal ring. A 1D closed nanotube results from coordination interactions between **TCBA³⁻** anions and **[NiL]²⁺** placed at adjacent tetragonal rings. Each nanotube is interpenetrated with four adjacent nanotubes to form a fivefold interlocked 3D framework. The resulting material, with 1D channels, exhibits highly selective adsorption of CO_2.

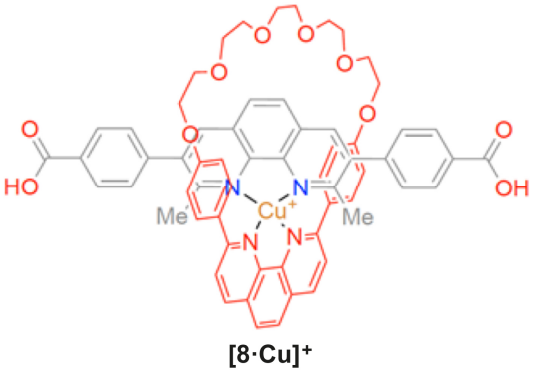

Fig. 18 Structure of **[8·Cu]⁺** acting as linker in **MORF-1040**.[79]

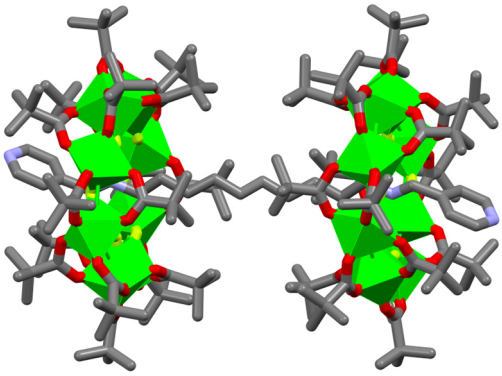

Fig. 19 Structure of [3]rotaxane **9**.[80] Hydrogen atoms are omitted for clarity. Colour key: red = oxygen atoms; grey = carbon atoms; blue = nitrogen atoms; yellow = fluorine atoms and green = chromium and nickel atoms.

2.2. Catenanes as ligands in metal-organic frameworks

[2]Catenanes[82] are mechanically interlocked molecules composed by two entwined macrocycles. The internal dynamics of these molecules is usually characterized by the rotational motion of their rings. This behaviour makes them very appealing candidates for participation as ligands in dynamics metal-organic frameworks. By inserting catenanes into a rigid and robust backbone, their movement could be potentially meaningful and coherent, even controllable.[36,82] In order to introduce [2]catenanes into MOFs, Yaghi, Stoddart and co-workers designed and synthesized a series of catenated struts.[83] These struts are made up of a linear rigid part that aims to build the robust backbone, and a crown ether macrocycle capable of establishing a mechanical bond with another wheel.

Stoddart, Yaghi and co-workers prepared **MOF-1011** using an interlocked strut, the first example of a metal-organic network bearing [2]catenanes.[84] The strut **10⁴⁺** (Fig. 21a) incorporates two rings stabilized by intermolecular π-π interactions: a bis-*p*-phenylene[34]-crown-10 (**BPP34C10**) and a tetracationic cyclophane cyclobis(paraquat-*p*-phenylene) (**CBPQT⁴⁺**). The triple bonds in the rigid part of the strut cause a small deviation from linearity, a not uncommon fact in polyines,[85] although in this case is a result of the steric hindrance from the interlocked rings. In addition, two terminal carboxylic acids at the crown ether allows the coordination to the metal ion. To synthesize **MOF-1011**, $Cu(NO_3)_2{\cdot}2.5H_2O$ and **10⁴⁺** are heated in a mixture of DMF, EtOH and H_2O.

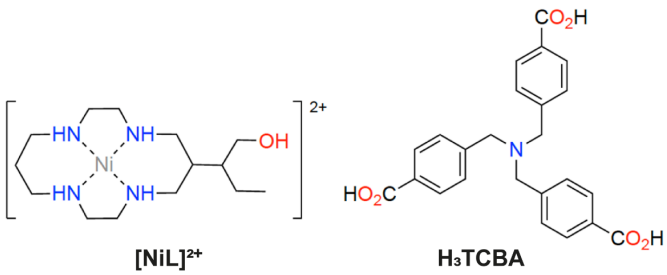

Fig. 20 Structures of **[NiL]²⁺** and **H₃TCBA**.[81]

The metal ion is reduced in the reaction, from copper(II) to copper(I), establishing three bonds with the organic strut, two with carboxylate groups from different ligands and other with one acetylenic fragment of a third strut in a η^2 way.

The X-ray structure of **MOF-1011** shows a 2D network (Fig. 21b,c). The macrocycles of the catenane are placed above and below the layer alternately, setting a zigzag sequence. Layers stack on the *b*-axis in an eclipsed fashion, triggering a shortening of the distance between the bipyridine unit and the hydroquinone fragment. As a result, **MOF-1011** has a high density of [2]catenanes in its structure (81 every 100 nm^2) with relatively good uniformity.

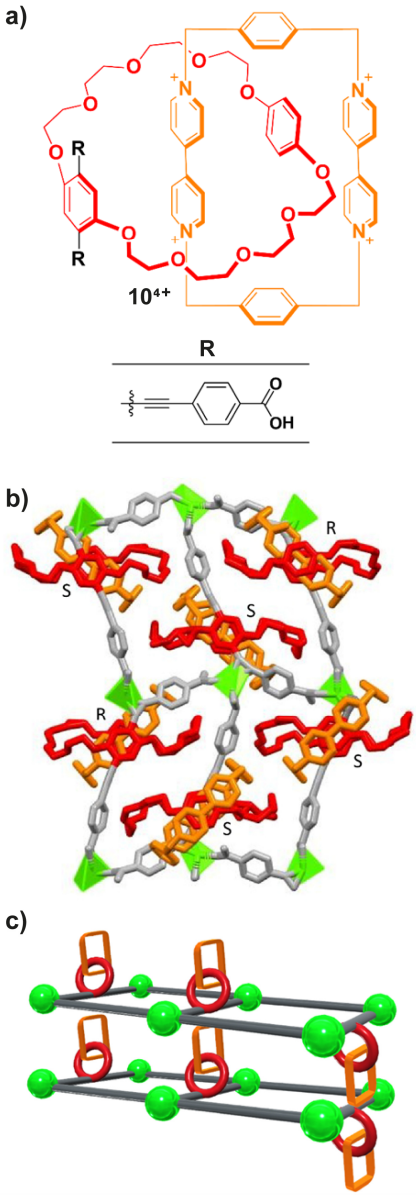

Fig. 21 (a) Chemical structure of the strut $\mathbf{10}^{4+}$; (b) stick representation of a 2D layer of **MOF-1011,** where the *R* or *S* configurations of the planar chirality of the catenanes are labelled; and (c) schematic sketch of a layer of **MOF-1011**.[84] Hydrogen atoms are omitted for clarity. Colour key: red = **BPP34C10**; orange = **CBPQT**$^{4+}$; grey = rigid part of the ligands; and green = copper atoms.

It is worth noting that equal numbers of molecules with (*R*) and (*S*) chiralities were identified in the reticular structure, rendering crystals racemic overall. Both enantiomers (*R* and *S*) come from the planar chirality that the organic strut initially presents. This chirality stems from the different arrangement of the bipyridine ring with respect to the hydroquinone in the strut.

Yaghi, Stoddart and co-workers went a step further and synthesized a three-dimensional metal-organic framework, **MOF-1030**.[86] For this purpose, the rigid strut was modified by increasing its length. Moreover, this change allowed the preparation of a network with larger pores, which could accommodate bulky [2]catenanes.

In this case, the crown ether used for the synthesis of the new strut $\mathbf{11}^{4+}$ is slightly different from that used in **MOF-1011**. A naphthalene unit replaced a hydroquinone fragment and, consequently, the size of the ring increased (Fig. 22a). The ligand consists of a naphthoparaphenylene[36]crown-10 (**NPP36C10**) and a cyclobis(paraquat-*p*-phenylene) (**CBPQT**$^{4+}$) rings intertwined one another. In order to increase the length of the rigid part of the strut, a longer chain of acetylenes and phenylenes was introduced (Fig. 22a). The corresponding carboxylic acids are located at the ends of this chain. The resulting strut also exhibits planar chirality as a consequence of the tetrasubstitution of the hydroquinone unit.

The synthesis of **MOF-1030** is similar to that of **MOF-1011**. Indeed, the copper atom established the same coordination bonds. However, the length of the chain causes a dramatic structural change. On the one hand, the π-conjugated system of the chain deteriorates as the phenylene rings deviated from the same plane. Some phenylene rings are almost orthogonal each other. On the other hand, a substantial topological change is observed. The metal ion environment becomes square-planar, placing two carboxylate groups and two carbon atoms from an acetylene motif at the vertex (Fig. 22b). This arrangement leads to a nearly perpendicular positioning of the carboxylate groups with respect the plane of the metal ion, thus leading to the three-dimensional network observed in **MOF-1030**. One of the most relevant features of this three-dimensional framework is that large pores are accessible to potentially recognize bulky target compounds, a property that could be useful for molecular storage.

The main drawback of **MOF-1011** and **MOF-1030**, was the η^2 bond between the metal ion and the acetylene group. To avoid the formation of this bond, Stoddart and co-workers replaced the acetylene groups in the rigid part of the strut with phenylene groups. In addition, a new non-degenerate tetracationic cyclophane was used to compare the structure obtained with that from the already known **CBPQT**$^{4+}$ macrocycle. As a result, they prepared two new materials, **MOF-1050** and **MOF-1051**,[87] in which seven phenylenes are inserted into the new rigid part of the strut. As usual, two carboxylic acids remain at the ends of the chain. The methyl group placed at the terminal phenylenes increases the solubility of the molecule. There are two variations in the macrocycles of the strut (Fig. 23a): $\mathbf{12a}^{4+}$ containing the interlocked rings of **NPP36C10** and **CBPQT**$^{4+}$; and $\mathbf{12b}^{4+}$, in which a bipyridine

(**BiPy**$^{2+}$) is substituted for a diazapyrenium (**DAP**$^{2+}$) on the tetracationic cyclophane ring. The interlocked struts **12a**$^{4+}$ and **12b**$^{4+}$ show stereoisomerism. Both the hydroquinone and naphthalene units placed at the crown ether macrocycle exhibit planar chirality. Depending on the absolute configuration of each unit, four stereoisomers could form the two diastereoisomeric pair of enantiomers (*RR*/*SS*) and (*RS*/*SR*). In the case of **12b**$^{4+}$, two additional translational isomers could also arise as result of which of the two cationic macrocycles, **BiPy**$^{2+}$ or **DAP**$^{2+}$, is encircled by the crown ether ring.

MOF-1050 and **MOF-1051** are synthesized under the above mentioned solvothermal conditions. Both metal-organic frameworks form two-dimensional layers arranged in the same way (Fig. 23b).

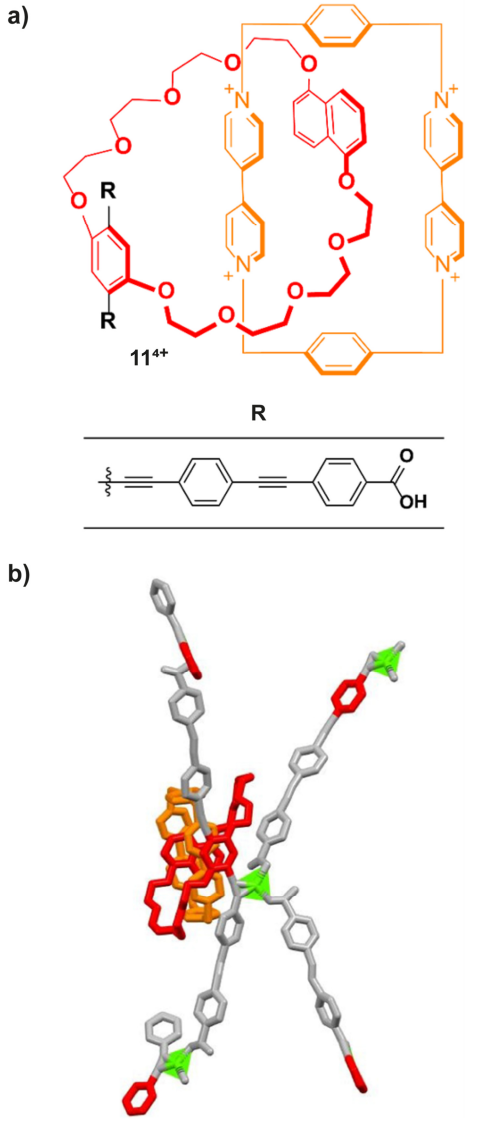

Fig. 22 (a) Structure of the strut **11**$^{4+}$; and (b) stick representation of the crystal structure of the bonds made by each copper atom in the **MOF-1030** lattice: two with carboxylate groups and one with an acetylene in a η^2 way.[86] Hydrogen atoms are omitted for clarity. Colour key: red = **NPP36C10**; orange = **CBPQT**$^{4+}$; grey = rigid part of the ligands; and green = copper atoms.

A copper paddlewheel cluster connects the struts by the coordination with the oxygens of four carboxylate groups. The X-ray structure of these materials shows that only the *RR* and *SS* enantiomeric pair of the organic struts leads to the successfully construction of these structures, turning out to be a stereoselective process. Moreover, in **MOF-1051**, synthesized with **12b**$^{4+}$, only the translational isomer that presents the DAP^{2+} inside the crown ether cavity is part of the crystalline array. Thus, in this later example a co-conformational selection process also takes place. This selectivity seems to be related to the molecular π-π stacking of catenanes in different layers of the metal-organic network. These weak interactions define the structure of the frameworks, perfectly self-selecting the adequate isomers to build the framework. The π-π stacking also causes the interpenetration between the **MOF-1050** layers, thus affording the resulting three-dimensional framework. The syntheses of **MOF-1050** and **MOF-1051** confirmed the strict diastereoselective control operating in the construction of these metal-organic networks. In addition, the intermolecular π-π stacking was shown to be a key factor for the structural arrangement of these materials.

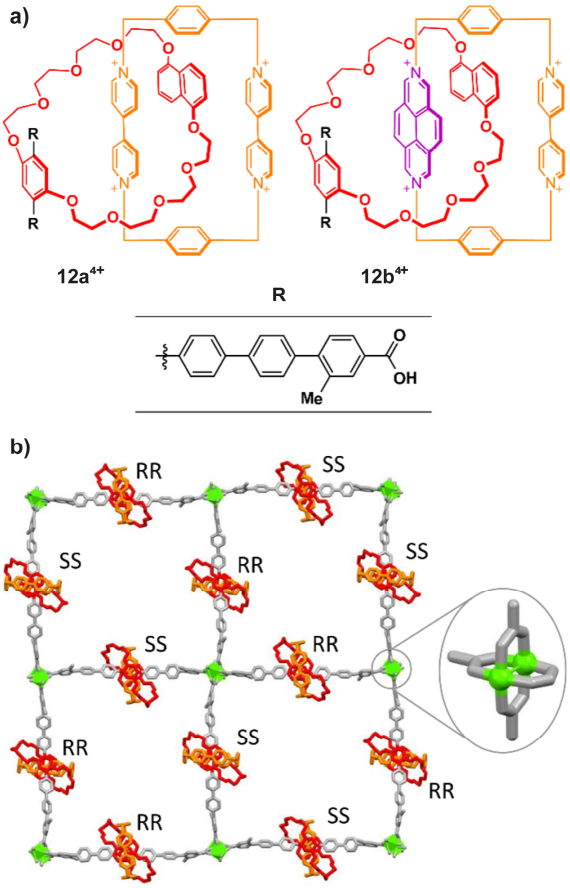

Fig. 23 (a) Chemical structure of the organic struts **12a**$^{4+}$ and **12b**$^{4+}$. The DAP^{2+} unit is coloured purple; and (b) stick representation of a single layer of **MOF-1050**, where the *RR* and *SS* enantiomers are labelled.[87] The ligands of the structure are bound by a copper paddlewheel. Hydrogen atoms are omitted for clarity. Colour key: red = **NPP36C10**; orange = **CBPQT**$^{4+}$; grey = rigid part of the ligands; and green = copper atoms.

In the examples shown so far, the motion of the [2]catenanes introduced into the metal-organic frameworks could not be controlled as there was no chance of a switchable motion between two well-defined stations promoted by an external stimulus. For this purpose, a desymmetrized [2]catenane capable of defining translational isomers must be integrated into the crystalline array, thus creating controllable switches.[88,89] External stimuli, usually chemical[90] or electronic,[91] could then induce mechanical movements causing changes in some observable properties to be detected (NMR, electrochemical potentials, electronic absorptions).

Stoddart and co-workers built a MOF incorporating a bistable [2]catenane.[92] In order to integrate this catenane with two well-defined states,[93] they radically changed the procedure for building these catenane-based materials. In contrast to the above examples, a previously synthesized metal-organic framework (**NU-1000**, Fig. 24a) was reacted with a [2]catenane (**13^{4+}**). The [2]catenane **13^{4+}** is not part of the organic strut, but a molecule that is introduced into the structure of a previously created network.

The bistable [2]catenane **13^{4+}** (Fig. 24b) consists of a polyether ring with two recognition sites, an electron-rich tetrathiafulvalene (TTF) station and a 1,5-dioxynaphthalene (DNP) unit. A **$CBPQT^{4+}$** ring is catenated to this macrocycle by donor-acceptor interactions. Also, the **$CBPQT^{4+}$** macrocycle was derivatized to incorporate a carboxylic acid at its end. This functional group is essential for the establishment of a coordination bond between the catenane and the **NU-1000** MOF.

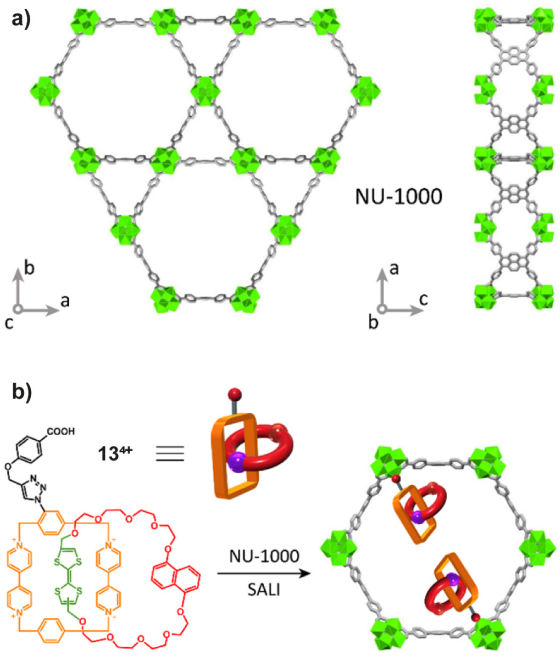

Fig. 24 (a) Crystal structure of the metal-organic framework **NU-1000**, where large pores are visible; and (b) synthesis of **NU-1000-13^{n+}** from the [2]catenane **13^{4+}** using the SALI protocol.[92] Colour key: red = **DNP** unit and crown ether ring; orange = **$CBPQT^{4+}$**; grey = the remaining part of the ligands; green = zirconium atoms and the reduced TTF station; and purple = the oxidised TTF station.

The 3D network of **NU-1000** is made up of 1,3,6,8-tetrakis(*p*-benzoic acid)pyrene (**TBApy**) linkers attached to metal clusters at the vertex (Fig. 24a). The metal clusters consist of six zirconium atoms coordinated to several hydroxy and oxo groups. Among the substituents attached to the metal ion, there are also some terminal OH groups and H_2O molecules. These ligands serve as coordination sites for the catenanes. As shown in Fig. 24a, the architecture of the **NU-1000** net shows hexagonal and triangular large pores, forming channels available for the accommodation of bulky molecules.

The incorporation of the catenane into the metal-organic network is based on the reaction between the terminal carboxylic acids of **13^{4+}** with the hydroxyl groups placed at the **NU-1000** nodes to obtain the new metal-organic framework **NU-1000-13^{n+}**. This efficient functionalization approach follows the SALI protocol (cited in section 2.1.6).[94] Solid-state UV-vis-NIR reflectance measurements were used to check the success of the reaction. Characteristic bands of charge transfer between the **$CBPQT^{4+}$** ring and the TTF station appeared to confirm the presence of the catenane ligand in the metal-organic material.

The number of [2]catenanes incorporated into the framework channels was another important issue to elucidate. Several experimental analyses combined with computational calculations were used for this purpose. The results showed that 0.65 equivalents of **13^{4+}** per node had been incorporated. Additionally, in each hexagonal pore, an average of two catenanes settled (Fig. 24b), while no catenanes were found in the triangular pores.

Aimed to test whether the bistable catenane integrated in **NU-1000-13^{n+}** was able to undergo a co-conformational switching, a redox cycle was performed, using 2,3-dichloro-5,6-dicyano-1,4-benzoquinone (DDQ) as the oxidizing agent, and ascorbic acid as the reducing agent. Both chemical reagents ensure that the only station susceptible to electron loss or gain is the TTF one. The **TBApy** linker and the **$CBPQT^{4+}$** macrocycle are also able to undergo redox exchanges, but not under these selected conditions. Solid-state UV-vis-NIR reflectance measurements were used to determine whether there is displacement between the two stations. When the oxidizing agent DDQ was used, the 800-1200 nm band was no longer observed in the spectrum. The result indicates the lack of charge transfer between the TTF station and the **$CBPQT^{4+}$** ring. This means that the TTF station is oxidised and leaves the **CBPQT** ring cavity by repulsion, with the DNP station taking its place. However, after treatment with ascorbic acid, the charge transfer band emerges again in the spectrum. This experiment proves that the mechanical motion of the bistable [2]catenane occurs inside of this reticular material.

The material **NU-1000-13^{n+}** is the first example of a MOF hosting a switchable bistable catenane.[92] This milestone brings us closer to the possibility of developing new molecular electronic devices[95] capable of acting as transistors[96], rectifiers[97], or solid-state molecular resistors.[98]

Recently, Aida, Sato and co-workers synthesized a MOF added to the group of materials bearing benzylic amide-based macrocycles[99,63] having exclusively [2]catenanes as organic ligands. Neither the construction of organic struts nor

previously synthesized MOFs was necessary. The macrocycles of the [2]catenanes themselves can coordinate to the metal ions to form the network. The result of this interesting architecture is a material capable of modifying its structure according to external stimuli, an elastic structure that marks an evolution in the synthesis of metal-organic frameworks.[100]

The interlocked ligand consists of two identical entangled benzylic amide macrocycles,[101–103] **14** (Fig. 25a). Both rings have two carboxylic acid groups placed at the isophthalamide fragments. These carboxylate groups allow the establishment of coordination bonds with four metal ions for building the polymer.

The metal-organic framework **^{CTN}MOF** is obtained by reaction between the [2]catenane **14** and cobalt(II) nitrate hexahydrate under solvothermal conditions. This methodology led to the formation of a crystalline array showing helical chirality (*M* helicity) of the ligands along the *a*-axis. In addition, the [2]catenanes exhibit a boat conformation, forming two pairs of hydrogen bonds between the benzylamide groups of the two interlocked rings (Fig. 25b), thus building a robust structure that displays a good thermal stability.

Notwithstanding, the ability of this metal-organic network to modify its structure according to the accommodation of hosts is its most remarkable property. The DMF-soaked **^{CTN}MOF** shows a specific PXRD pattern that disappears when this solvent is removed from its channels. If the network is soaked in another solvent such as acetonitrile or ethanol, the original pattern also disappears, registering different ones. Nevertheless, when the structure is immersed in DMF again, the initial PXRD pattern is recovered. Therefore, the structure changes its morphology depending on the molecule that hosts inside its pores. This phenomenon does not only occur with host solvents, but also at different temperatures. For example, at room temperature the lattice shows a tetragonal arrangement, while an orthorhombic morphology is observed at -180 °C.

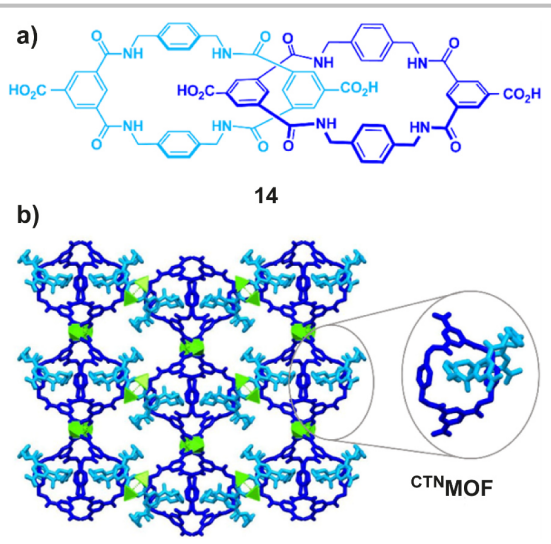

Fig. 25 (a) Chemical structure of the [2]catenane **14** consisting of two intertwined benzylic amide macrocycles; and (b) crystal structure of **^{CTN}MOF**.[100] Hydrogen atoms are omitted for clarity. Colour key: blue = benzylic amide macrocycles; and green = cobalt atoms.

The nanoindentation technique, which is a hardness test, allowed to determine the elasticity of **^{CTN}MOF** through the calculation of the Young's modulus. When air-dried **^{CTN}MOF** is evaluated with this technique, the observed Young's modulus is 6.3 GPa. However, if the framework is soaked in DMF, the Young's modulus decreases to 1.8 GPa, being the most elastic metal-organic crystal ever recorded. To put these data in context, rubber has a Young's modulus between 0.01 and 0.1 GPa, while for iron this value is 210 GPa.[104] The improvement in elasticity of **^{CTN}MOF** is due to the attenuation of hydrogen bonds caused by DMF. Compared to other materials, **^{CTN}MOF** is on a par with the well-known polypropylene (1.5-2.0 GPa).[104]

The preparation of **^{CTN}MOF** is relevant to address the issue of porous materials where the release of high-affinity guest molecules is difficult to achieve. Thus, the construction of a squeezable MOF is possible if the elastic properties can be further improved by a rational design of the interlocked strut.

3. Dynamics in metal-organic rotaxane frameworks

Mechanically interlocked molecules show an incoherent motion in solution, due to their random dispersion, that needs to be controlled for developing a useful function. The incorporation of rotaxanes into a material is a requirement to exploit their operability at the macroscopic level. For this operation, MIMs must have enough space in the material to allow the dynamics of its diverse components. Metal-organic frameworks constitute an ideal support for the integration of dynamic intertwined ligands. The utilization of rotaxanes as organic ligands in MOFs has led to large-amplitude motions, including rotation and translation, at the macroscopic level.[26] The random motion of the intertwined components observed in solution is restricted when the interlocked ligands are well-organized in the crystalline array. Consequently, the incorporation of rotaxanes within the rigid architectures of MOFs should substantially enhance the order, coherence and performance of the motion, affording a material with robust dynamics.[36]

3.1. Rotational motion of rotaxanes incorporated in MOFs

The rotational motion of rotaxanes has been deeply studied in solution,[105–111] but only a scarce number of examples in the solid state have been reported so far. In close analogy to the study of the rotational motion of non-interlocked rotors[112,113] and motors[114,115] in MOFs, the characterization of the dynamics of the rotational motion in MORFs is performed by solid state ^{2}H-NMR measurements of isotopically-labelled surrogates. Also, in rotaxane-based MOFs, the study of the resulting powder patterns at different temperatures, highly responsive to molecular motion, is the preferred spectroscopic technique.[25]

In 2012, Loeb and co-workers disclosed the preparation of the first MORF which showed internal dynamics, named as **UWDM-1** (Fig. 26).[116] The interlocked ligand **15** is constituted of a [24]crown-6 macrocycle, labelled with two deuterium atoms, surrounding a benzylaniline-based thread. The coordination of the carboxylate groups, placed at the stoppers of the thread, to

four different copper(II) paddlewheel clusters afforded a metal-organic material having an overall formula of $[Cu_2(\mathbf{15})(H_2O)_2]\cdot 3H_2O$. The cyclic component of the intertwined linker can rotate around the linear component as the material has enough void volume. The dynamics of the macrocycles within the MOF was studied by variable temperature (VT) solid state ^{2}H-NMR spectroscopy, showing a dense array of rotating crown-ether-based macrocycles, with a strong dependence on the temperature. The reversible removal of the water molecules from the copper(II) paddlewheels and the pores by heating at 150 °C under reduced pressure increased the void space, allowing the rotational motion to take place. Resolvation with water, which stablishes hydrogen bonds with the macrocycles, prevents the wheel dynamics. Thus, the rotational motion of the cyclic components can experience on/off cycles (activation/deactivation) without deformation of the crystalline lattice.

Insightful studies on related systems demonstrated that variations on the size of the macrocycle interfere on the material dynamics.[117] By using [22]crown-6, [26]crown-6 and benzo[24]crown-6-based rotaxane linkers, the preparation of isomorphous MORFs with different degrees of motion of the wheel (dependent of the temperature) was accomplished. VT solid state ^{2}H-NMR studies revealed that the material showing higher dynamics turned out to be the MORF bearing [24]crown-6 macrocycles, indicating that the incorporation of linkers with these cyclic components confers enough free volume, limiting the interactions between the threads and the wheels inside the network.

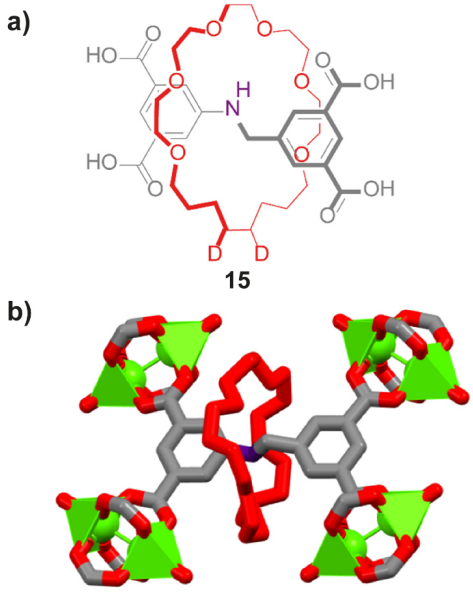

Fig. 26 (a) Chemical structure of rotaxane **15**, and (b) stick representation of the single-crystal structure of **UWDM-1** showing a single unit of the interlocked ligand **15** coordinated to four different copper(II) paddlewheels.[116] Hydrogen atoms and axial water molecules are omitted for clarity. Colour key: red = [24]crown-6 and oxygen atoms; grey = benzylaniline thread; purple = nitrogen atoms; and green = copper atoms.

Loeb, Schurko and co-workers prepared a dynamic zinc organic framework using a [24]crown-6 macrocycle encircling a bipyridine-based thread and 4,4'-biphenyldicarboxylic acid (BPCD) as ligands.[118] This material, named **UWDM-3**, builds two-periodic grids connecting the carboxylate ligands with the zinc(II) paddlewheel clusters having the mechanically interlocked bipyridine pillaring different layers (Fig. 27a).

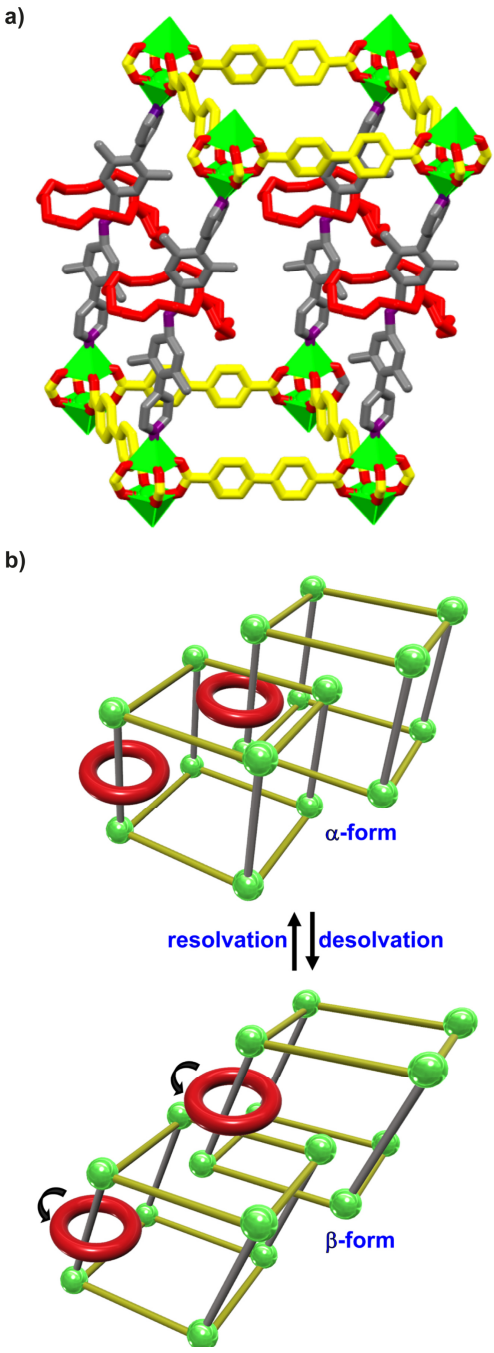

Fig. 27 (a) Stick representation of the single-crystal structure of **UWDM-3** showing a portion of lattice framework; and (b) cartoon representation illustrating the reversible phase conversion between α-form (solvated) and β-form (desolvated).[118] Hydrogen atoms and interpenetration are omitted for clarity in the solid structure. Colour key: red = [24]crown-6 and oxygen atoms; yellow = BPCD ligand; grey = bipyridine threads; purple = nitrogen atoms; and green = zinc atoms.

Aimed to characterize the mobility of the rings inside this MORF, the deuterium labelled material was prepared and probed by solid state ^{2}H NMR. The as-synthesized **UWDM-3** shows a solvated phase with restricted rotational motion (α-form) (Fig. 27b, above). Through heating or solvent exchange with dichloromethane, a phase transition is promoted by a desolvation process. In the desolvated phase of the MOF (β-form phase), the wheels of the pillared MIM struts have enough free volume to experience full rotation (Fig. 27b, below).

The reversibility of the phase change by desolvation/resolvation cycles allows to switch the MIM dynamics in the solid state. The reversible phase transitions in MOFs bearing pillaring rotaxanes have also been studied by employing porphyrinic-based tetradentate planar linkers. Two different rotaxanes, **16** and **17**, having respectively pyridine and 2-picoline rings at the ends of the threads (Fig. 28a), were used to prepare these materials. The reaction of these interlocked pillars and a palladium porphyrin-based tetracarboxylate linker with $Zn(NO_3)_2{\cdot}6H_2O$ afforded two different MOFs, **UWDM-6** and **UWDM-7**.[119]

Both materials adopt a 2-fold interpenetrated *fsc* net with the porphyrins forming two dimensional metallogrids connected through the zinc(II) paddlewheels and the [2]rotaxanes pillars linking the different grids (Fig. 28b). Through solvent removal, a reversible phase change takes places, allowing a partial rotational motion of the wheels in the different states of **UWDM-6** (R = H), although without significant alterations of the ^{2}H NMR powder patterns.

On the other hand, in the α-form of **UWDM-7** (R = Me), a rapid onset of the two-site jump motion and a full rotational motion are observed by increasing the temperature or by performing different solvent exchanges in the pores. The desolvation of this MORF afforded the β-phase, which combines a two-site jump and a partial rotation of the wheel.

The phase transition induced by a stimulus has been also applied to topologically rigid MOFs prepared with non-interlocked linkers. Such reticular systems show a breathing phenomenon of the pores,[120] converting, for example, insulator materials into conductor ones[121] or generating frustrated flexible hybrid MOFs,[122] among others. The upcoming of the design of MIMs-containing MOFs with reversible phase changes could be focused on these intriguing behaviours for getting flexible and functional dynamic MOFs.

The use of imidazolium-based threads surrounded by [24]crown-6 ether macrocycles as organic ligands satisfyingly led to the preparation of diverse Zn-containing MOFs (**UWDM-5**) having a wide range of conformational exchanges and full rotational motions, even at low temperatures, as it was proved by ^{2}H NMR spectroscopy in the solid state.[123] At high temperature, the dynamics of these MOFs is similar to that of the previously reported interlocked aniline-based materials.[116,117] Similar to those, isoreticular copper(II)-based MOFs with non-interlocked (**UWCM-14**) and interlocked (**UWDM-14**) T-shaped benzimidazole struts have also been prepared (Fig. 29).[124]

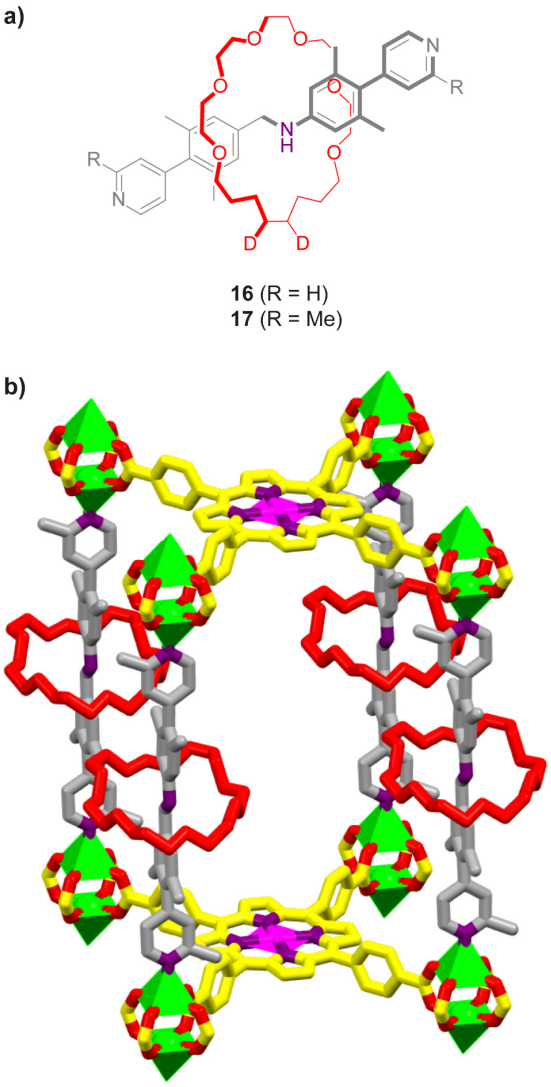

16 (R = H)
17 (R = Me)

Fig. 28 (a) Chemical structure of rotaxanes ligands of **16** and **17**; and (b) stick representation of the single-crystal structure of **UWDM-7** showing a single lattice framework.[119] Hydrogen atoms and interpenetration are omitted for clarity. Colour key: red = [24]crown-6 and oxygen atoms; yellow = porphyrinic ligands; grey = bipyridine threads; purple = nitrogen atoms; green = zinc atoms; and magenta = palladium atoms.

This approach allowed a comparative study between MOFs showing the same net, with or without the presence of the mechanical bond. The wheels in the resulting *lil* nets[125] showed in the solid state the same types of motions (rocking, partial rotation and full rotation) previously studied in solution. This example illustrates a rational design of a MOF presenting robust dynamics by using reticular synthesis.

In most of the reported examples of dynamics in MIMs struts within MOFs, the rotational motion is attributed to the cyclic component, whereas the threads remain fixed to the reticular network. The relative rotation of intertwined amide-based threads having carboxylate groups placed at the wheel has also been studied in this type of functional porous materials.[63] This example will be discuss in detail later (see Section 4.2).

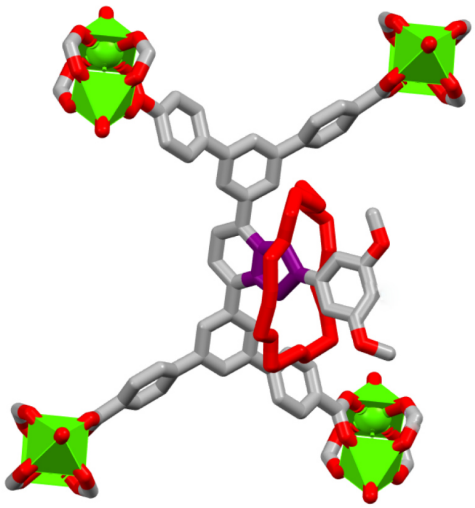

Fig. 29 Stick representation of the single-crystal structure of **UWDM-14** showing an interlocked benzimidazole connected to four different copper(II) paddlewheel clusters.[124] Hydrogen atoms are omitted for clarity. Colour key: red = [24]crown-6 and oxygen atoms; grey = carbon atoms of the thread; purple = benzimidazole moiety; and green = copper atoms.

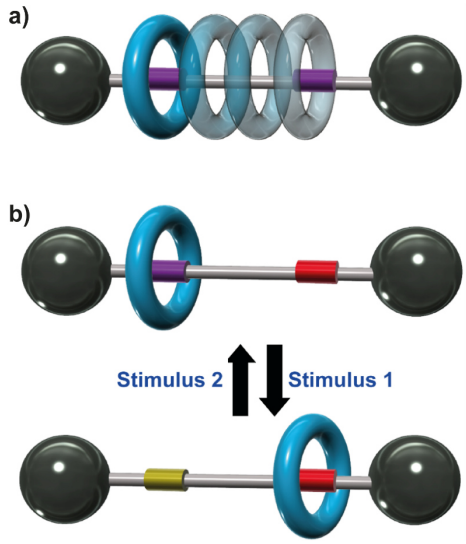

Fig. 30 Cartoon representation of: (a) a degenerate molecular shuttle; and (b) a non-degenerate molecular shuttle. Colour key: purple = higher affinity station; red = intermediate affinity station; yellow = lower affinity station; black = stoppers; grey = thread; and blue = macrocycle.

To date, key milestones have been achieved in this area but there is still much to discover. Future research should be focused on the application of the broad knowledge of postsynthetic functionalization of crystalline arrays[126] to study variations on the rotational dynamics of the interlocked parts, by inducing affinities similar to those observed in solution.[108,127]

3.2. Translational motion of rotaxanes incorporated into MOFs

The control of the translational motion between the different components present in a rotaxane-based structure has captured attention of scientists working in the area of molecular machinery.[16,17] Rotaxane-based molecular shuttles are systems with various binding sites at the linear component, named as stations, that interact with the cyclic counterpart. When the binding sites have equivalent energies, no switch over the position of the wheel is possible (degenerate system) (Fig. 30a).[128–130] The positional preference of the macrocycle along the thread is possible by a rational design of the molecular shuttle. Thus, a non-degenerate (also named as bistable) system can be prepared by incorporating stations with different affinities for the macrocycle (Fig. 30b).

The switching of the shuttling motion is possible by changing the affinity order of the stations as a response to the application of an external stimulus.[131–135] The ideal scenario is that enabling a full control of the position of the cyclic component along the thread.

In solution, the positional integrity (or population level of the macrocycle) over a station shows a clear dependence on the used solvent. In this regard, competitive solvents can limit the interaction between the cyclic and linear components or even preclude its establishment. The incorporation of molecular shuttles in a condensed phase, such as a MOF, reduces this limitation and can allow greater precision in the shuttling switch.

The Loeb's research group has significantly contributed to the development of this field. The first example of the use of degenerate molecular shuttles as linkers for the preparation of metal-organic frameworks was reported in 2015.[136,137] The resulting MORF named **UWDM-4**, is constituted by a symmetrical thread that includes two undistinguishable benzimidazole stations, as a connecting unit between two polyphenyl-based dicarboxylate struts, surrounded by a [24]crown-8 macrocycle (Fig. 31a). The dicarboxylic units are coordinated to different Zn_4O clusters forming a cubic lattice. The network owns the adequate free void volume to allow the wheel motions (Fig. 31b). The imidazole moieties of the mechanically interlocked ligands were ^{13}C-enriched to study the translational motion by using VT solid state ^{13}C-NMR spectroscopy. At high temperatures (318-334 K), a single peak at 154.0 ppm was observed in the solid state NMR spectra. At 298 K, this peak splits into two different resonances with chemical shifts of 152.7 and 152.2 ppm. The Eyring plot built with the NMR data determined a shuttling rate of the [24]crown-8 macrocycle along the axle, inside the crystalline array, of 283 s^{-1} at 298 K with an activation barrier ($\Delta G^{\ddagger}$) of 14.1 kcal·mol^{-1} ($\Delta H^{\ddagger}$ = 15.4 kcal·mol^{-1}; $\Delta S^{\ddagger}$ = 4.3 cal·mol^{-1}·K^{-1}). A slower translational rate was observed in the solid state in comparison to that obtained in solution, by using the tetramethyl ester rotaxane precursor of the ligand ($\Delta G^{\ddagger}$ = 7.7 kcal·mol^{-1}; $\Delta H^{\ddagger}$ = 13.0 kcal·mol^{-1}; $\Delta S^{\ddagger}$ = 17.7 cal·mol^{-1}·K^{-1}).

The higher activation barrier in the solid state can be explained by the presence of the rigid framework that induces steric and electrostatic hindrances to the shuttling motion. The lower activation entropy determined in **UWDM-4** arises from the restriction in the number of possible configurations due to the lack of solvent interactions with the MIMs ligands, in contrast with what occurs in solution.

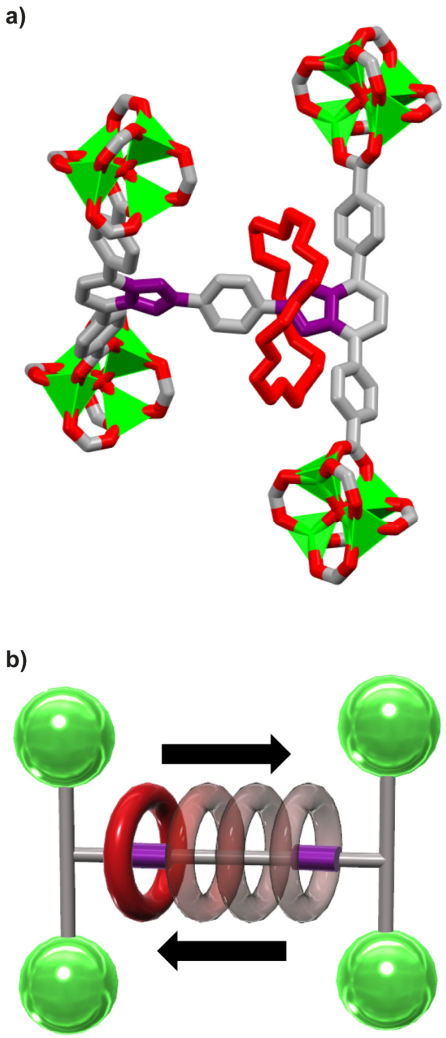

Fig. 31 (a) Stick representation of the crystal structure of **UWDM-4** showing a [24]crown-6-based molecular shuttle functionalized with two benzimidazole stations coordinated to four zinc(II) paddlewheel clusters through carboxylate groups placed at the stoppers; and (b) cartoon representation of the shuttling motion of **UWDM-4**.[137] Hydrogen atoms are omitted for clarity. Colour key: red = [24]crown-8 and oxygen atoms; grey = carbon atoms of the thread; purple = benzimidazole; and green = zinc atoms.

The requirement of a cooperative motion of multiple wheels inside the crystalline array could be another explanation of the lower activation entropy value observed in the solid state. Thus, the shuttling of a macrocycle would force the translational motion of the neighbouring wheels. This example[137] demonstrated for the first time that the dynamics of molecular shuttles with rotaxane structures could operate inside MOF scaffolds.

4. Stimuli-responsive metal-organic rotaxane frameworks

The control of the internal dynamics of mechanically interlocked molecules, incorporated into a solid framework, by the action of an external stimulus remains highly challenging. One of the most important issues to overcome in this field is the lack of addressability of all the interlocked systems placed in the inner of the material. As a result, the dynamics of only a fraction of ligands can be modulated. Moreover, the stability of the crystal framework must be considered[138,139] when a certain stimulus is applied for switching the motion of the wheel in molecular-shuttle linkers. To date, only a few stimuli-responsive MOFs with rotaxane-based linkers have been described.

4.1. Redox-responsive MORFs

In 2015, Stoddart and collaborators successfully functionalized the premade MOF **NU-1000**[140] with pseudorotaxanes.[77] By following the post-synthetic SALI protocol they were able to chemically modify the inner of the pores. The substitution of the non-bridging OH groups and H_2O molecules from the Zn clusters, oriented towards the channels, was easily achieved in an ordered manner. Thus, a trisradical semirotaxane **18**$^{\bullet+}$⊂**CBPQT**$^{2(\bullet+)}$ (Fig. 32a), instantaneously formed upon reduction of a benzoic acid-functionalized viologen-containing derivative **18** and the cyclophane **CBPQT**,[141] coordinated to the Zn clusters (Fig. 32b). This protocol allows the obtention of a robust dynamic material. Each channel trapped up to three threads, from which half of them, in average, are encircled by a macrocycle forming the MIM species (the Zn cluster acts as the second stopper to stabilize the mechanical bond). Electrochemical studies of a thin film of the SALI-modified MOF were performed. When a negative potential (-250 mV) was applied, a semireversible reduction wave was observed, attributable to the viologen components confined within the channels. The current flow across the SALI-modified material revealed that 43% of the viologen units were electrochemically accessible, and therefore, their dynamics are modulated by this input. Inspired by this successful approach, a bistable catenane was post-synthetically integrated[92] in **NU-1000** (see Fig. 24b) which also kept the redox-switching properties of its mechanical unit in the solid state (see Section 2.2).

4.2. Light-responsive MORFs

Fumaramide-based threads have been extensively used for the assembly of hydrogen-bonded rotaxanes.[105,130,142] The light-induced isomerization of interlocked fumaramides to the corresponding maleamides is widely employed for the control of the internal dynamics (rotational and translational motions).[143,144] Berna and co-workers incorporated the fumaramide rotaxane ***E*-19** (Fig. 33a), having two carboxylic acids attached to the macrocycle, as organic linker for the construction of a photoresponsive MIM-containing Cu-based metal-organic framework, named as **UMUMOF-(*E*)-3** (Fig. 33b).[63] Starting from the maleamide-based linker, the synthesis of the **UMUMOF-(*Z*)-3** was also accomplished.

By means of solid state ^{2}H NMR experiments, the internal dynamics of the deuterated interlocked olefins inside the frameworks were analysed. In solution, the rotational barriers found for the maleamide-based rotaxanes are much lower than that of their fumaramide analogues. In the solid state, the maleamide threads also exhibits a faster motion inside the network of **UMUMOF-(*Z*)-3** than those of the fumaramide threads in **UMUMOF-(*E*)-3**, although with minor variations.

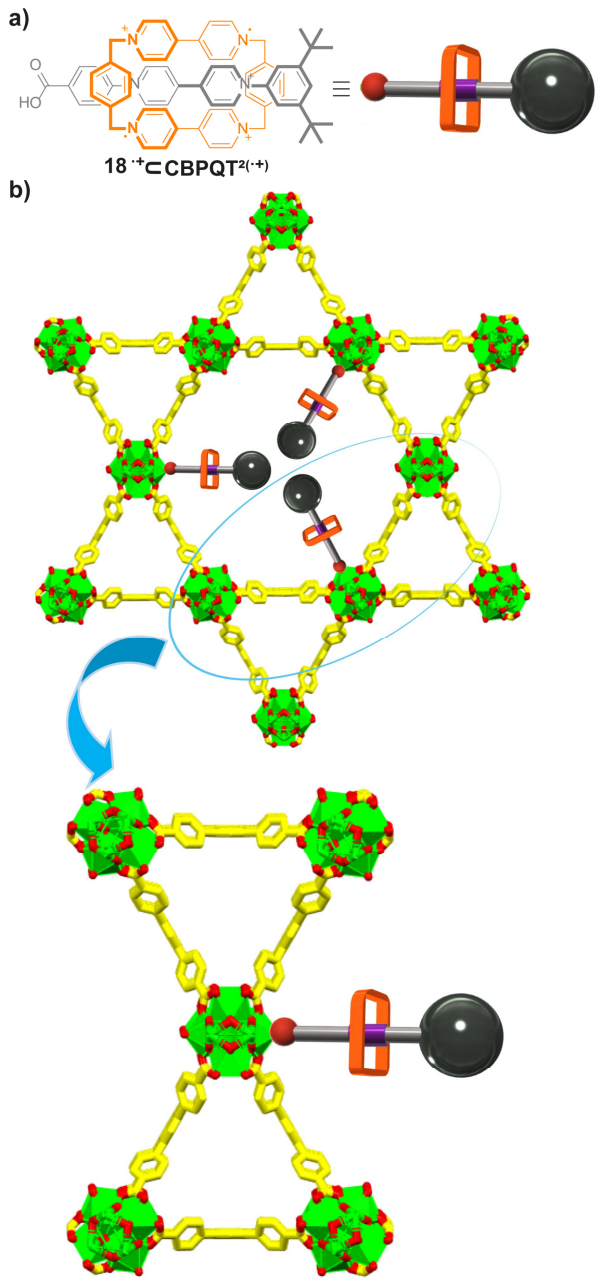

Fig. 32 (a) Chemical structure of the semirotaxane **18**$^{\cdot+}$**⊂CBPQT**$^{2(\cdot+)}$ and its cartoon representation; and (b) stick representation of the single-crystal X-ray structure of MOF **NU-1000** having CBPQT-based rotaxanes grafted to zirconium clusters (incorporated with a graphical software).[77] Colour key: red = oxygen atoms; grey = carbon atoms of the thread; purple = benzimidazole moiety; yellow = non-interlocked linkers; orange = CBPQT macrocycle; black = stoppers; and green = zinc atoms.

These results indicate that the rotational motion of the organic linkers inside the rigid network is noticeably dampened. Nevertheless, upon irradiation at 312 nm of **UMUMOF-(*E*)-3**, 20% of the fumaramide-based linkers are isomerized to their maleamide isomers thus yielding the material **UMUMOF-($E_{80}Z_{20}$)-3**.

Similarly, a similar percentage of maleamide linkers are transformed into fumaramides when the **UMUMOF-(*Z*)-3** is irradiated. As a consequence of the isomerization of the interlocked threads present at these materials, the available free volume into the channels varies. This particular way for controlling the size of the voids of these MOFs allows its utilization as controllable containers (Fig. 33c).

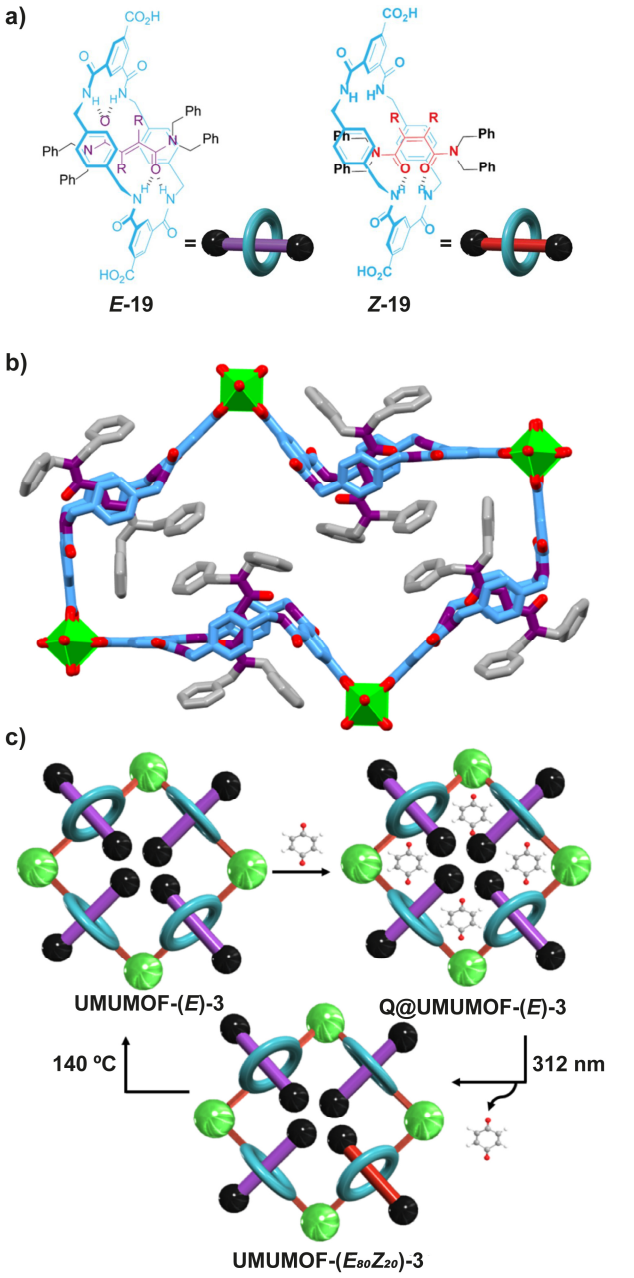

Fig. 33 (a) Structure of the interlocked ligands ***E*-19** (R = H, D) and ***Z*-19** (R = H, D) and their cartoon representations; (b) stick representation of the crystal structure of **UMUMOF-(*E*)-3** showing a rhombohedral framework comprising four copper paddlewheel clusters and four fumaramide-based rotaxanes. Colour key: red = oxygen atoms and maleamide; grey = carbon atoms; purple = fumaramide; blue = tetralactam macrocycle; and green = copper atoms; and (c) cyclic working of the **UMUMOF-(*E*)-3** as dispenser of *p*-benzoquinone **(Q)**, involving three steps: cargo loading, photorelease and thermal recovery.[63]

When the *p*-benzoquinone-loaded material **UMUMOF-(*E*)-3** is irradiated, the delivery of the cargo was triggered. The isomerization of the fumaramide units varies the volume of the pores in a breathing-like phenomenon, liberating the quinone. The material can be reutilized isomerizing the maleamide units by a thermal treatment. The load and release can be repeated up to three cycles, retaining an 80% of its cargo capacity.

4.3. pH- and solvent responsive MORFs

One straightforward method for switching in solution the shuttling process of crown ether-based rotaxanes such as the interlocked bis(benzimidazole) **20** (Fig. 34a) is the variation of the pH.[145,146] The neutral or charged interlocked species resulting from a change of the hydronium concentration have very different activation barriers and translational rates. For the application of this stimuli in a MIM-containing MOF, a highly stable framework is required. For this mission, zirconium(IV) organic frameworks are privileged candidates due to their excellent thermal, chemical and mechanical stabilities.[146] Loeb and colleagues doped the Zr-based **UiO-68** and **PCN-57**, having triphenylene dicarboxylate (**TPDC**, Fig. 34b) and tetramethyl-triphenylene dicarboxylate (**TTDC**, Fig. 34b) linkers, respectively, with a [24]crown-8-based H-shaped tetracarboxylate molecular shuttle **20**.[147]

These new MOFs, **UWDM-8** and **UWDM-9**, were expected to have an analogous structure to that of **PCN-57**, in which the edges of the tetrahedral cavities are composed by four **TTDC** (or **TPDC** linker in **UiO-68**) and two ^{13}C-enriched mechanically interlocked organic ligands. The molecular-shuttle linker **20** is constituted by a thread with two benzimidazole stations, having a biphenyl spacer unit, surrounded by a [24]crown-8 wheel. In the network, **20** is coordinated through its triphenyl-dicarboxylate stoppers to the $Zr_6(OH)_4O_4$ clusters (Fig. 34c).

To test the pH stability of these new materials, the as-synthesized MOFs were treated with a strong base proton sponge and trifluoromethanesulfonic acid. PXRD and scanning electron microscopy/energy-dispersive X-ray spectroscopy corroborated the structural integrity of the crystalline array after the acid/base cycles. The study of the shuttling motion of the tetramethyl ester precursors, analogous of the interlocked tetracarboxylate linkers, showed a reduction of the translational rate at low pH values, when the diprotonation of the benzimidazole stations occurs.

The translational motion of the molecular shuttles inside the zirconium-based MOFs was also evaluated by using VT solid state ^{13}C-NMR. These studies revealed that the [24]crown-8 macrocycle in the neutral **UWDM-8** is locked into one of the stations due to the steric hindrance provided by the methyl groups of the **TTDC** linkers. The lack of the methyl groups in the **TPDC** linkers of **UWDM-9** seems to point out that the translational ring motion between the benzimidazole stations might occur but it could not be unequivocally corroborated by solid state NMR measurements as the interactions with the rotor-like linkers make difficult a conclusive analysis in this particular case (for subsequent studies of similar materials see Section 5).[147]

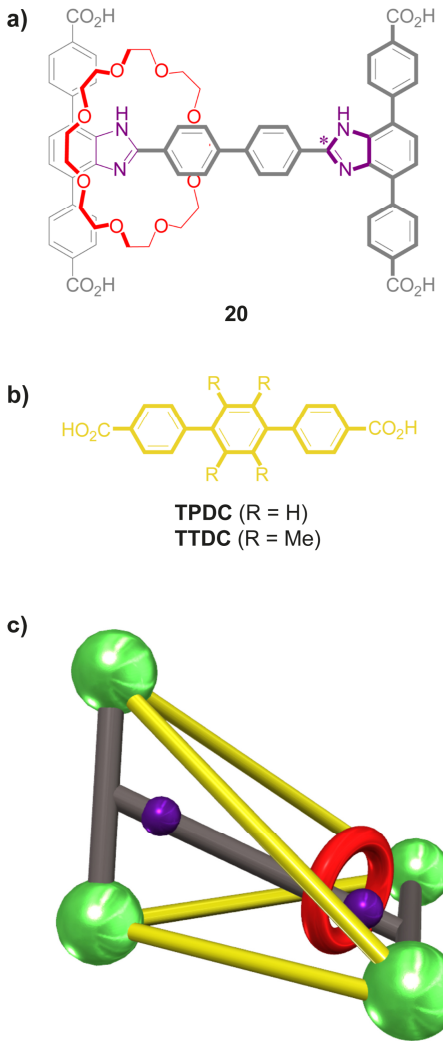

Fig. 34 (a) Chemical structure of the interlocked linker **20** incorporated into **UWDM-8** and **UWDM-9**; (b) chemical structure of **TPDC** and **TTDC** linkers; and (c) cartoon representation of **UWDM-8** integrating **TTDC** linkers and **UWMD-9** integrating **TPDC** linkers.[147] Colour key: red = [24]crown-8; grey = carbon atoms of the thread; purple = benzimidazole moiety; yellow = **TPDC** or **TTDC** linkers; and green = zirconium atoms; * = ^{13}C-enriched atom.

By incorporating a non-degenerate molecular shuttle as organic linker, the same research group reported the preparation of the zirconium-based MOF **UWDM-11**.[148] The bistable molecular shuttle is constituted by a thread having two different benzimidazole stations, one functionalized with two bromine atoms and another with two pendant phenyl-carboxylate moieties, encircled by a [24]crown-8 cyclic component. The X-ray single-crystal structure of the interlocked ligand shows that the wheel preferentially surrounds the station attached to the phenyl dicarboxylate groups (Fig. 35a). This [2]rotaxane, along with **TTDC** linkers, was employed to prepare a **PCN-57** related MOF, **UWDM-11** (Fig. 35b), having a rotaxane:**TTDC** ratio of 1:8. This ratio indicates that the appended crown ether-based molecular shuttle occupied almost a 95% of the octahedral cavities of the framework. The benzimidazole rings of the thread are ^{13}C enriched at the 2-position to support the characterisation of the translational motion of the wheel by using VT solid state ^{13}C NMR.

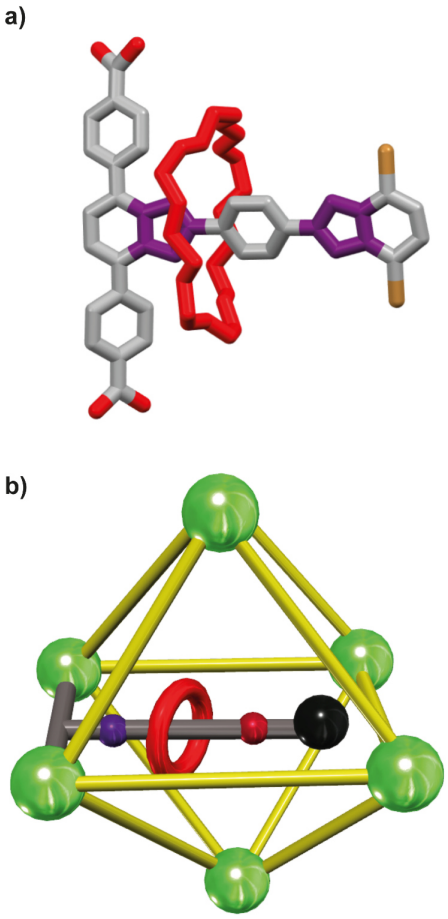

Fig. 35 (a) Chemical structure of the molecular shuttle linker incorporated into **UWDM-11**; and (b) cartoon representation of **UWMD-11**.[148] Colour key: red = [24]crown-8; grey = carbon atoms of the thread; purple = terphenyl-stoppered benzimidazole moiety; maroon = dibromide-functionalized benzimidazole moiety; yellow = **TTDC** linkers; brown = bromide atoms; and green = zirconium atoms.

The non-degenerate linker in **UWDM-11** has two chemically different stations, the terphenyl stoppered station **A** and the dibromo stoppered station **B**. The solid state ^{13}C NMR spectra of neutral **UWMD-11** (after deprotonation by treatment with a proton sponge), having mesitylene guest molecules between the octahedral cavities and the empty tetrahedral cavities, revealed that the macrocycle is mainly placed over the station **A** at 173 K (78% of positional integrity). As expected for a non-degenerated molecular shuttle, the system shows two different translational rates. For this mesitylene-filled MORF at the coalescence temperature (273 K), the station **A** to station **B** transition occurs at 162.3 s^{-1} whereas the exchange from benzimidazole **B** to **A** proceeds at 575.3 s^{-1}. The translational motion of the ring between these two stations was shown to be notably faster when it occurs in a fully activated **UWDM-11** having solvent-free cavities.[148] This remarkable research paves the way for the development of MOF-based devices bearing binary molecular switches that can operate by applying an external stimulus in order to invert the thermodynamic positional preference of the [24]crown-8 wheels. Although a complete study about the control of the internal motions was not fully accomplished, these materials can be considered as pH-responsive systems. During the MOF synthesis, the protonated benzimidazolium recognition sites strongly interact with the crown ether macrocycle. Under these conditions, no molecular shuttling is expected to occur in the solid state, as happened in solution with shuttles of this type,[149,150] although this study was not overcome. Thus, the variation of the pH of the bulk can triggered a change on the rate of the translational motions inside the ordered materials.

4.4. Far-from-equilibrium working using mechanized MOFs materials

An innovative approach to incorporate MIMs into arrayed materials have been recently reported by Stoddart and co-workers, by introducing the concept of active mechanisorption.[151,152] A series of pumping cassettes (**MPCG**)[153] are grafted to a surface of 2D MOF nanosheets, inducing the out-of-equilibrium incorporation of wheels on their collecting chains.

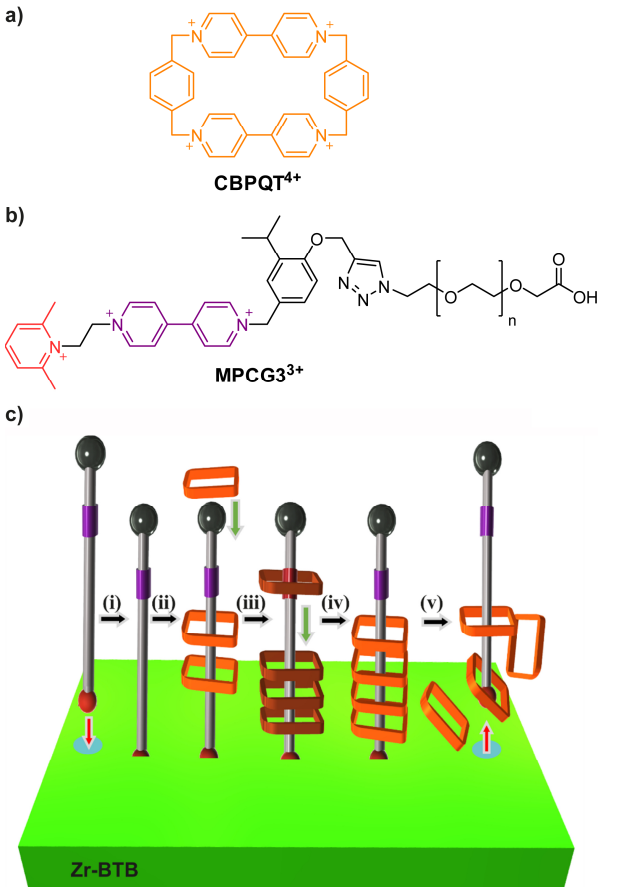

Fig. 36 (a) Chemical structure of **CBPQT**$^{4+}$; (b) chemical structure of **MPCG3**$^{3+}$ showing the **DiMePy**$^{+}$ and **BiPy**$^{2+}$ motifs in red and purple, respectively; and (c) cartoon representation of the mechanisorption mechanism: (i) grafting of **MPCG3** on the 2D MOF nanosheets; (ii) redox-driven adsorption of wheels; (iii) reduction-driven threading of wheels through the pumping cassette; (iv) oxidation-driven repulsion of the wheels from the pumping cassette; and (v) acid-triggered desorption of wheels due to the cleavage of the coordination bonds between the MOF surface and **MPCG3**.[151]

In contrast with the previously described MORFs in which the mechanical operations, rotation or translational movements, occur inside the frameworks, artificial molecular pumps operate at the surface of an ultrathin MOF nanosheet-based material. By introducing modified pumping cassettes, they developed high-capacity mechanisorption systems, in which multiple macrocycles can be stored in each pump (Fig. 36). For this goal, carboxyl-terminated molecular pumps **MPCG3**$^{3+}$ (with a redox switchable station bipyridinium (**BiPy**$^{2+}$) and a Coulombic barrier 2,6-dimethylpyridinium (**DiMePy**$^{+}$) were incorporated to a layered Zr-BTB framework (**BTB** for 4,4',4''-benzene-1,3,5-triyl-tris(benzoic acid) linker) (Fig. 36, i and ii). Upon electrochemical reduction, the **BiPy**$^{2+}$ units are reduced to the radical cation **BiPy**$^{\cdot+}$, triggering the threading of the cyclobis(paraquat-*p*-phenylene) rings **CBPQT**$^{2(\cdot+)}$, able to easily overcome the steric barrier of **DiMePy** and formed strong radical-radical interactions with the **BiPy**$^{\cdot+}$ station (Fig. 36, iii). After oxidation, the repulsion between the **BiPy**$^{2+}$ and **DiMePy**$^{+}$ with the oxidized ring **CBPQT**$^{4+}$ forces the macrocycles to move to the collection chain of the pump (Fig. 36, iv). By following this procedure, the material $\mathbf{Zr_6(MPCG1)_{0.4}(CBPQT)_{0.4}}$ was isolated. The desorption of the wheels and the pump can be achieved by acid treatment, without compromising the integrity of the MOF (Fig. 36, v). This breakthrough approach allows the storage of energy in form of chemical gradients, showing a great potential for future applications of chemical capacitators in technology.

5. Coupled individual motions of rotaxane-based MOFs

Loeb, Schurko and collaborators took one step more in the complexity of dynamic MOFs. They were able to study the internal dynamics of MOFs with two mobile components: a rigid rotor and a crown-ether rotaxane.[154,155] This work was based on the design of the reported **PCN-57**-based MOFs, **UWDM-8** and **UWDM-9**.[147] The phenylene-type rings are widely used for the preparation of molecular rotors.[112,113,156–158] The coexistence of phenylene molecular rotors with degenerate bistable molecular shuttles inside the MOF network could result in interferences between the motions of both organic linkers. [24]Crown-8 macrocycles, surrounding a ^{13}C-labeleded H-shaped biphenyl thread, were inserted into the tetrahedral cavities of the **PCN-57**-type MOFs (Fig. 37a). Primary **TTDC**, **TPDC-*d*$_4$** or diphenyldicarboxy-tetrazine (**DPCT**) linkers spanned each of the tetrahedral cavities in MOFs **UWDM-8**, **UWDM-9-*d*$_4$** and **UWDM-10**, respectively. The dynamics of the non- and interlocked linkers were evaluated by using VT solid state ^{13}C-NMR. These experiments showed an orthogonal position of the sterically hindered **TTDC** linker at the edge of the tetrahedral cavities within **UWDM-8**, in which the interlocked strut prevented any possible motion of the wheel (Fig. 37b). The flattering disposition of the less sterically demanding tetrazine rings in the non-interlocked linkers of **UWDM-10** allows the motion of the cyclic component of the molecular shuttle (Fig. 37c).

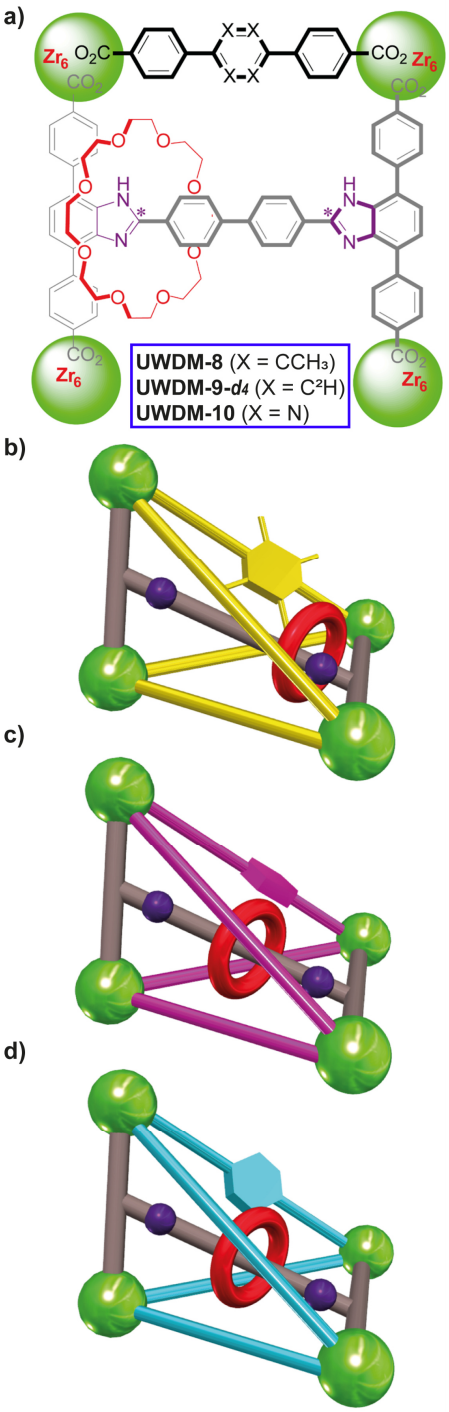

Fig. 37 (a) General diagram of the series of synthesized zirconium(IV)-based MOFs showing the chemical structure of the molecular shuttle and terphenylene-type struts; (b) cartoon representation of **UWDM-8** having tetramethylphenylene units at the edges of the tetrahedral cavity (macrocycle locked); (c) cartoon representation of **UWDM-10** having tetrazine units at the edges of the tetrahedral cavity (macrocycle unlocked); and (d) cartoon representation of **UWDM-9-*d*$_4$** having tetradeuterophenylene units at the edges of the tetrahedral cavity (correlated motion of the macrocycle).[155] Colour key: red = [24]crown-8; grey = carbon atoms of the thread; purple = benzimidazole moiety; yellow = tetramethylphenylene-based struts; magenta = tetrazine-based struts; blue = tetradeuterophenylene-based struts and green = zirconium atoms; * = ^{13}C-enriched atom.

Interestingly, the tetradeuterated **TPDC** struts of **UWDM-9-*d*$_4$** could experience a rotational motion which turned out to be coupled with the shuttling of the [24]crown-8 wheel of the interlocked linkers (Fig. 37d). This work was a pioneering example of cooperatively functioning molecular machines and an exceptional case of molecular crosstalk inside of a reticular material.

6. Summary and outlook

The incorporation of MIMs within MOFs brings the opportunity to translate the properties conferred by the mechanical bond to condensed phase materials. Up to now, some synthetic achievements have been accomplished, focused on the use of intertwined organic ligands in the preparation of MOFs and the functionalization of prefabricated MOFs with mechanically interlocked motifs. Furthermore, some systems which preserve the dynamics of the MIM components and their switching behaviour have been developed. The preparation of MOFs using rotaxanes is today better established than that using catenanes. Indeed, only a few examples of MOFs containing catenanes have been reported so far.

In order to employ the promising properties of these emerging materials, some general research directions should be addressed in this burgeoning area. Besides the use of new types of interlocked struts, one of the main objectives is to increase the structural complexity of the MIM ligands to prepare metal-organic materials having enhanced properties. For example, the utilization of interlocked catalysts[159–163] ligands would open new possibilities in heterogeneous catalysis using MOFs.[11] Very likely, recent developments on the preparation of enantiopure MIMs incorporating novel chirality motifs[164–166] would spot significant advances in the construction of coherent chiral MOFs which can be employed in asymmetric catalysis. Other applications of intertwined molecules that have been widely studied in solution, in the context of molecular sensing[167] or ring-activated transformations,[168] could play an interesting role in the operability and usability of MOF-based materials.

The future of the research focused on the integration of molecular shuttles into MOFs should be directed to the assembly of stimuli-responsive materials by incorporating different affinity sites into the mechanically interlocked ligands. As examples, new networks incorporating photoactive stations, such as fumaramides, pyridyl-acyl hydrazones or azobenzenes,[131,132,169] could emerge as potential solid state photoresponsive devices. Aimed to develop an advanced generation of controllable materials, the challenging incorporation of more complex systems, such as molecular lassos or daisy chain rotaxanes,[170–174] inside the network would also be tackled. The contraction/expansion of these linkers, mimicking the muscle motions,[172,175] would drastically modify the properties of these materials by changing the dimensions of the internal channels, and thus of the entire crystalline array. Regarding the switchable materials, the combination of the flexible properties of catenane-based MOFs and the control over its rotational motion could lead to smart breathing materials which might be useful in the development of advanced molecular dispensers.

The increase of control over the construction of MOF with multiple structural domains would be also useful to couple the motion of different dynamic interlocked and non-interlocked systems in the pursuit of emerging intricate molecular factories.[115]

Despite the encouraging results reported to date, there are still some issues to overcome. More precise and sensitive analytical methods must be developed to determine the morphological changes of the materials caused by the switching of the mechanical motions. Furthermore, the stability of the MOF backbones must withstand the conditions employed for triggering a change of the dynamics without causing damage to the crystalline array. The stimuli should be also able to induce a response in all the interlocked units incorporated into the material, at the surface and at the inner of the pores. The ideal scenario is to get an identical operability at the surface and at the interior of the crystalline material, like that observed in solution.

MIMs-based MOFs have an interesting present and a promising future in the preparation of smart materials. One of the most attractive aspects for chemists in this area is the great variety of conceivable structural designs. The possibilities of functionalization both in the cyclic and the linear counterparts, as well as the wide availability of a plethora of metallic salts and clusters, leaves the imagination of the scientist as the only limitation.

Conflicts of interest

There are no conflicts to declare.

Acknowledgements

This work was supported by the MICINN (PID2020-113686GB-I00/MICIN/AEI/10.13039/501100011033) and Fundacion Seneca-CARM (Project 20811/PI/18). A. Saura-Sanmartin and G. Cutillas-Font thank Fundacion Seneca-CARM for their contracts (20259/FPI/17 and 21442/FPI/20). A. Saura-Sanmartin also thanks Ministerio de Universidades of the Government of Spain for his Margarita Salas postdoctoral contract (financed by the European Union – NextGenerationEU).

Notes and references

1 M. O'Keeffe, M. A. Peskov, S. J. Ramsden and O. M. Yaghi, *Acc. Chem. Res.*, 2008, **41**, 1782–1789.

2 N. W. Ockwig, O. Delgado-Friedrichs, M. O'Keeffe and O. M. Yaghi, *Acc. Chem. Res.*, 2005, **38**, 176–182.

3 A. Schneemann, V. Bon, I. Schwedler, I. Senkovska, S. Kaskel and R. A. Fischer, *Chem. Soc. Rev.*, 2014, **43**, 6062–6096.

4 R. Freund, S. Canossa, S. M. Cohen, W. Yan, H. Deng, V. Guillerm, M. Eddaoudi, D. G. Madden, D. Fairen-Jimenez, H. Lyu, L. K. Macreadie, Z. Ji, Y. Zhang, B. Wang, F. Haase, C. Wöll, O. Zaremba, J. Andreo, S. Wuttke and C. S. Diercks, *Angew. Chem. Int. Ed.*, 2021, **60**, 23946–23974.

5 R. Freund, O. Zaremba, G. Arnauts, R. Ameloot, G. Skorupskii, M. Dincă, A. Bavykina, J. Gascon, A. Ejsmont, J. Goscianska, M. Kalmutzki, U. Lächelt, E. Ploetz, C. S. Diercks

and S. Wuttke, *Angew. Chem. Int. Ed.*, 2021, **60**, 23975–24001.
6 Y. Li and J. Yu, *Nat. Rev. Mater.*, 2021, **6**, 1156–1174.
7 Z. Ji, H. Wang, S. Canossa, S. Wuttke and O. M. Yaghi, *Adv. Funct. Mater.*, 2020, **30**, 2000238.
8 J. Hwang, A. Ejsmont, R. Freund, J. Goscianska, B. V. K. J. Schmidt and S. Wuttke, *Chem. Soc. Rev.*, 2020, **49**, 3348–3422.
9 M. Eddaoudi, D. B. Moler, H. Li, B. Chen, T. M. Reineke, M. O'Keeffe and O. M. Yaghi, *Acc. Chem. Res.*, 2001, **34**, 319–330.
10 H. Li, K. Wang, Y. Sun, C. T. Lollar, J. Li and H. C. Zhou, *Mater. Today*, 2018, **21**, 108–121.
11 A. Bavykina, N. Kolobov, I. S. Khan, J. A. Bau, A. Ramirez and J. Gascon, *Chem. Rev.*, 2020, **120**, 8468–8535.
12 M. J. Kalmutzki, C. S. Diercks and O. M. Yaghi, *Adv. Mater.*, 2018, **30**, 1704304.
13 W. Xu and O. M. Yaghi, *ACS Cent. Sci.*, 2020, **6**, 1348–1354.
14 D. Sluysmans and J. F. Stoddart, *Trends Chem.*, 2019, **1**, 185–197.
15 C. J. Bruns and J. F. Stoddart, *The Nature of the Mechanical Bond: From Molecules to Machines*, John Wiley & Sons, Inc., Hoboken, NJ, USA, 2016.
16 S. Erbas-Cakmak, D. A. Leigh, C. T. McTernan and A. L. Nussbaumer, *Chem. Rev.*, 2015, **115**, 10081–10206.
17 I. Aprahamian, *ACS Cent. Sci.*, 2020, **6**, 347–358.
18 A. W. Heard and S. M. Goldup, *ACS Cent. Sci.*, 2020, **6**, 117–128.
19 D. A. Leigh, *Angew. Chem. Int. Ed.*, 2016, **55**, 14506–14508.
20 J. F. Stoddart, *Angew. Chem. Int. Ed.*, 2017, **56**, 11094–11125.
21 J. P. Sauvage, *Angew. Chem. Int. Ed.*, 2017, **56**, 11080–11093.
22 B. L. Feringa, *Angew. Chem. Int. Ed.*, 2017, **56**, 11060–11078.
23 S. Mena-Hernando and E. M. Pérez, *Chem. Soc. Rev.*, 2019, **48**, 5016–5032.
24 S. J. Loeb, *Chem. Soc. Rev.*, 2007, **36**, 226–235.
25 P. Martinez-Bulit, A. J. Stirk and S. J. Loeb, *Trends Chem.*, 2019, **1**, 588–600.
26 B. H. Wilson and S. J. Loeb, *Chem*, 2020, **6**, 1604–1612.
27 O. M. Yaghi, *ACS Cent. Sci.*, 2019, **5**, 1295–1300.
28 J.-K. Sun, L.-X. Cai, Y.-J. Chen, Z.-H. Li and J. Zhang, *Chem. Commun.*, 2011, **47**, 6870–6872.
29 X.-T. Zhang, D. Sun, B. Li, L.-M. Fan, B. Li and P.-H. Wei, *Cryst. Growth Des.*, 2012, **12**, 3845–3848.
30 X.-L.- Wang, N. Han, H.-Y. Lin, C. Xu, J. Luan and G.-C. Liu, *Bull. Korean Chem. Soc.*, 2012, **33**, 3793–3796.
31 W. Bury, D. Fairen-Jimenez, M. B. Lalonde, R. Q. Snurr, O. K. Farha and J. T. Hupp, *Chem. Mater.*, 2013, **25**, 739–744.
32 N. Zhu, M. J. Lennox, G. Tobin, L. Goodman, T. Düren and W. Schmitt, *Chem. - Eur. J.*, 2014, **20**, 3595–3599.
33 X. Wang, J.-Y. Luo, J.-W. Tian, D.-D. Huang, Y.-P. Wu, S. Li and D.-S. Li, *Inorg. Chem. Commun.*, 2018, **98**, 141–144.
34 K. Lu, A. Liebman Peláez, L. Wu, Y. Cao, C. H. Zhu and H. Fu, *Inorg. Chem.*, 2019, **58**, 1794–1805.
35 K. Kim, *Chem. Soc. Rev.*, 2002, **31**, 96–107.
36 H. Deng, M. A. Olson, J. F. Stoddart and O. M. Yaghi, *Nat. Chem.*, 2010, **2**, 439–443.
37 K. Zhu and S. J. Loeb, *Top. Curr. Chem.*, 2014, **354**, 213–251.
38 D. Whang, Y.-M. Jeon, J. Heo and K. Kim, *J. Am. Chem. Soc.*, 1996, **118**, 11333–11334.
39 D. Whang, J. Heo, C.-A. Kim and K. Kim, *Chem. Commun.*, 1997, 2361–2362.
40 K. M. Park, D. Whang, E. Lee, J. Heo and K. Kim, *Chem. - Eur. J.*, 2002, **8**, 498–508.
41 D. Whang and K. Kim, *J. Am. Chem. Soc.*, 1997, **119**, 451–452.
42 E. Lee, J. Heo and K. Kim, *Angew. Chem. Int. Ed.*, 2000, **39**, 2699–2701.
43 J. Liang, X.-L. Wang, Y.-Q. Jiao, C. Qin, K.-Z. Shao, Z.-M. Su and Q.-Y. Wu, *Chem. Commun.*, 2013, **49**, 8555–8557.
44 X.-S. Wu, J. Liang, X.-L. Hu, X.-L. Wang, B.-Q. Song, Y.-Q. Jiao and Z.-M. Su, *Cryst. Growth Des.*, 2015, **15**, 4311–4317.
45 J. Liang, X.-S. Wu, X.-L. Wang, C. Qin, K.-Z. Shao, Z.-M. Su and R. Cao, *CrystEngComm*, 2016, **18**, 2327–2336.
46 X.-S. Wu, X.-L. Wang, F.-L. Zhu, H.-F. Bao, C. Qin and Z.-M. Su, *Chem. Commun.*, 2018, **54**, 5474–5477.
47 X.-S. Wu, H.-F. Bao, F.-L. Zhu, J. Sun, X.-L. Wang and Z.-M. Su, *Dalton Trans.*, 2019, **48**, 9939–9943.
48 X. S. Wu, D. M. Cheng, X. L. Wang, J. Sun, H. Y. Zang and Z. M. Su, *Dalton Trans.*, 2020, **49**, 1747–1751.
49 X. Yang, M. Giorgi, H. Karoui, D. Gigmes, V. Hornebecq, O. Ouari, A. Kermagoret and D. Bardelang, *Chem. Commun.*, 2019, **55**, 13824–13827.
50 J.-K. Sun and J. Zhang, *Dalton Trans.*, 2015, **44**, 19041–19055.
51 X.-D. Zhang, Y. Zhao, K. Chen, X.-Y. Dao, Y.-S. Kang, Y. Liu and W.-Y. Sun, *Chem. - Eur. J.*, 2020, **26**, 2154–2158.
52 S. J. Loeb and J. A. Wisner, *Angew. Chem. Int. Ed.*, 1998, **37**, 2838–2840.
53 S. J. Loeb and J. A. Wisner, *Chem. Commun.*, 1998, 2757–2758.
54 S. J. Loeb, *Chem. Commun.*, 2005, 1511–1518.
55 G. J. E. Davidson and S. J. Loeb, *Angew. Chem. Int. Ed.*, 2003, **42**, 74–77.
56 V. N. Vukotic and S. J. Loeb, *Chem. Soc. Rev.*, 2012, **41**, 5896–5906.
57 D. J. Mercer, J. Yacoub, K. Zhu, S. K. Loeb and S. J. Loeb, *Org. Biomol. Chem.*, 2012, **10**, 6094–6104.
58 D. J. Hoffart and S. J. Loeb, *Supramol. Chem.*, 2007, **19**, 89–93.
59 D. J. Hoffart and S. J. Loeb, *Angew. Chem. Int. Ed.*, 2005, **44**, 901–904.
60 L. K. Knight, V. N. Vukotic, E. Viljoen, C. B. Caputo and S. J. Loeb, *Chem. Commun.*, 2009, 5585–5587.
61 V. N. Vukotic and S. J. Loeb, *Chem. - Eur. J.*, 2010, **16**, 13630–13637.
62 D. J. Mercer, V. N. Vukotic and S. J. Loeb, *Chem. Commun.*, 2011, **47**, 896–898.
63 A. Saura-Sanmartin, A. Martinez-Cuezva, D. Bautista, M. R. B. Marzari, M. A. P. Martins, M. Alajarin and J. Berna, *J. Am. Chem. Soc.*, 2020, **142**, 13442–13449.
64 N. C. Frank, D. J. Mercer and S. J. Loeb, *Chem. - Eur. J.*, 2013, **19**, 14076–14080.

65 G. Gholami, K. Zhu, J. S. Ward, P. E. Kruger and S. J. Loeb, *Eur. J. Inorg. Chem.*, 2016, 4524–4529.

66 G. Gholami, G. Baggi, K. Zhu and S. J. Loeb, *Dalton Trans.*, 2017, **46**, 2462–2470.

67 H. Y. Gong, B. M. Rambo, W. Cho, V. M. Lynch, M. Oh and J. L. Sessler, *Chem. Commun.*, 2011, **47**, 5973–5975.

68 H. Y. Gong, B. M. Rambo, C. A. Nelson, V. M. Lynch, X. Zhu and J. L. Sessler, *Chem. Commun.*, 2012, **48**, 10186–10188.

69 X.-L. Chen, Y.-J. Shen, C. Gao, J. Yang, X. Sun, X. Zhang, Y.-D. Yang, G.-P. Wei, J.-F. Xiang, J. L. Sessler and H.-Y. Gong, *J. Am. Chem. Soc.*, 2020, **142**, 7443–7455.

70 Y.-D. Yang, C.-C. Fan, B. M. Rambo, H.-Y. Gong, L.-J. Xu, J.-F. Xiang and J. L. Sessler, *J. Am. Chem. Soc.*, 2015, **137**, 12966–12976.

71 T. Xia, Z.-Y. Yu and H.-Y. Gong, *Molecules*, 2021, **26**, 4241.

72 Q. Li, W. Zhang, O. S. Miljanić, C.-H. Sue, Y.-L. Zhao, L. Liu, C. B. Knobler, J. F. Stoddart and O. M. Yaghi, *Science*, 2009, **325**, 855–859.

73 C. Valente, E. Choi, M. E. Belowich, C. J. Doonan, Q. Li, T. B. Gasa, Y. Y. Botros, O. M. Yaghi and J. F. Stoddart, *Chem. Commun.*, 2010, **46**, 4911–4913.

74 N. L. Strutt, D. Fairen-Jimenez, J. Iehl, M. B. Lalonde, R. Q. Snurr, O. K. Farha, J. T. Hupp and J. F. Stoddart, *J. Am. Chem. Soc.*, 2012, **134**, 17436–17439.

75 P. Deria, W. Bury, J. T. Hupp and O. K. Farha, *Chem. Commun.*, 2014, **50**, 1965–1968.

76 M. Kim, J. F. Cahill, H. Fei, K. A. Prather and S. M. Cohen, *J. Am. Chem. Soc.*, 2012, **134**, 18082–18088.

77 P. R. McGonigal, P. Deria, I. Hod, P. Z. Moghadam, A.-J. Avestro, N. E. Horwitz, I. C. Gibbs-Hall, A. K. Blackburn, D. Chen, Y. Y. Botros, M. R. Wasielewski, R. Q. Snurr, J. T. Hupp, O. K. Farha and J. F. Stoddart, *Proc. Natl. Acad. Sci. U. S. A.*, 2015, **112**, 11161–11168.

78 M.-X. Wu, J. Gao, F. Wang, J. Yang, N. Song, X. Jin, P. Mi, J. Tian, J. Luo, F. Liang and Y.-W. Yang, *Small*, 2018, **14**, 1704440.

79 A. Coskun, M. Hmadeh, G. Barin, F. Gándara, Q. Li, E. Choi, N. L. Strutt, D. B. Cordes, A. M. Z. Slawin, J. F. Stoddart, J.-P. Sauvage and O. M. Yaghi, *Angew. Chem. Int. Ed.*, 2012, **51**, 2160–2163.

80 G. F. S. Whitehead, B. Cross, L. Carthy, V. A. Milway, H. Rath, A. Fernandez, S. L. Heath, C. A. Muryn, R. G. Pritchard, S. J. Teat, G. A. Timco and R. E. P. Winpenny, *Chem. Commun.*, 2013, **49**, 7195–7197.

81 P. Ju, L. Jiang and T. B. Lu, *Chem. Commun.*, 2013, **49**, 1820–1822.

82 G. Gil-Ramírez, D. A. Leigh and A. J. Stephens, *Angew. Chem. Int. Ed.*, 2015, **54**, 6110–6150.

83 Y.-L. Zhao, L. Liu, W. Zhang, C.-H. Sue, Q. Li, O. S. Miljanić, O. M. Yaghi and J. F. Stoddart, *Chem. - Eur. J.*, 2009, **15**, 13356–13380.

84 Q. Li, W. Zhang, O. S. Miljanic, C. B. Knobler, J. F. Stoddart and O. M. Yaghi, *Chem. Commun.*, 2010, **46**, 380–382.

85 O. Š. Miljanić, W. R. Dichtel, S. I. Khan, S. Mortezaei, J. R. Heath and J. F. Stoddart, *J. Am. Chem. Soc.*, 2007, **129**, 8236–8246.

86 Q. Li, C.-H. Sue, S. Basu, A. K. Shveyd, W. Zhang, G. Barin, L. Fang, A. A. Sarjeant, J. F. Stoddart and O. M. Yaghi, *Angew. Chem. Int. Ed.*, 2010, **49**, 6751–6755.

87 D. Cao, M. Juríček, Z. J. Brown, A. C. H. Sue, Z. Liu, J. Lei, A. K. Blackburn, S. Grunder, A. A. Sarjeant, A. Coskun, C. Wang, O. K. Farha, J. T. Hupp and J. F. Stoddart, *Chem. - Eur. J.*, 2013, **19**, 8457–8465.

88 V. Balzani, M. Gómez-López and J. F. Stoddart, *Acc. Chem. Res.*, 1998, **31**, 405–414.

89 J. P. Sauvage, *Acc. Chem. Res.*, 1998, **31**, 611–619.

90 V. Balzani, A. Credi, S. J. Langford, M. Raymo, J. F. Stoddart and M. Venturi, *J. Am. Chem. Soc.*, 2000, **122**, 3542–3543.

91 C. P. Collier, G. Mattersteig, E. W. Wong, Y. Luo, K. Beverly, J. Sampaio, F. M. Raymo, J. F. Stoddart and J. R. Heath, *Science*, 2000, **289**, 1172–1175.

92 Q. Chen, J. Sun, P. Li, I. Hod, P. Z. Moghadam, Z. S. Kean, R. Q. Snurr, J. T. Hupp, O. K. Farha and J. F. Stoddart, *J. Am. Chem. Soc.*, 2016, **138**, 14242–14245.

93 M. Asakawa, P. R. Ashton, V. Balzani, A. Credi, C. Hamers, G. Mattersteig, M. Montalti, A. N. Shipway, N. Spencer, J. F. Stoddart, M. S. Tolley, A. J. P. White and D. J. Williams, *Angew. Chem. Int. Ed.*, 1998, **37**, 333–337.

94 P. Deria, J. E. Mondloch, E. Tylianakis, P. Ghosh, W. Bury, R. Q. Snurr, J. T. Hupp and O. K. Farha, *J. Am. Chem. Soc.*, 2013, **135**, 16801–16804.

95 A. Coskun, J. M. Spruell, G. Barin, W. R. Dichtel, A. H. Flood, Y. Y. Botros and J. F. Stoddart, *Chem. Soc. Rev.*, 2012, **41**, 4827–4859.

96 A. C. Whalley, M. L. Steigerwald, X. Guo and C. Nuckolls, *J. Am. Chem. Soc.*, 2007, **129**, 12590–12591.

97 G. Ho, J. R. Heath, M. Kondratenko, D. F. Perepichka, K. Arseneault, M. Pézolet and M. R. Bryce, *Chem. - Eur. J.*, 2005, **11**, 2914–2922.

98 T. Lee, W. Wang, J. F. Klemic, J. J. Zhang, J. Su and M. A. Reed, *J. Phys. Chem. B*, 2004, **108**, 8742–8750.

99 A. Saura-Sanmartin, A. Martinez-Cuezva, M. Marin-Luna, D. Bautista and J. Berna, *Angew. Chem. Int. Ed.*, 2021, **60**, 10814–10819.

100 W. Meng, S. Kondo, T. Ito, K. Komatsu, J. Pirillo, Y. Hijikata, Y. Ikuhara, T. Aida and H. Sato, *Nature*, 2021, **598**, 298–303.

101 A. G. Johnston, D. A. Leigh, L. Nezhat, J. P. Smart and M. D. Deegan, *Angew. Chem. Int. Ed. Engl.*, 1995, **34**, 1212–1216.

102 M. S. Deleuze, D. A. Leigh and F. Zerbetto, *J. Am. Chem. Soc.*, 1999, **121**, 2364–2379.

103 D. H. Li and B. D. Smith, *Beilstein J. Org. Chem.*, 2019, **15**, 1086–1095.

104 Engineering ToolBox. Young's Modulus, Tensile Strenght and Yield Strenght Values for Some Materials, https://www.engineeringtoolbox.com/young-modulus-d_417.html, (accessed April 2022).

105 F. G. Gatti, S. León, J. K. Y. Wong, G. Bottari, A. Altieri, M. A. F. Morales, S. J. Teat, C. Frochot, D. A. Leigh, A. M. Brouwer and F. Zerbetto, *Proc. Natl. Acad. Sci. U. S. A.*, 2003, **100**, 10–14.

106 I. Poleschak, J. M. Kern and J. P. Sauvage, *Chem. Commun.*, 2004, 474–476.

107 P. Liu, X. Shao, C. Chipot and W. Cai, *Chem. Sci.*, 2016, **7**, 457–462.

108 A. Saura-Sanmartin, J. S. Martinez-Espin, A. Martinez-Cuezva, M. Alajarin and J. Berna, *Molecules*, 2017, **22**, 1078.

109 Q. W. Zhang, J. Zajíček and B. D. Smith, *Org. Lett.*, 2018, **20**, 2096–2099.

110 H. V. Schröder, A. Mekic, H. Hupatz, S. Sobottka, F. Witte, L. H. Urner, M. Gaedke, K. Pagel, B. Sarkar, B. Paulus and C. A. Schalley, *Nanoscale*, 2018, **10**, 21425–21433.

111 S. Amirjalayer, A. Martinez-Cuezva, J. Berna, S. Woutersen and W. J. Buma, *Angew. Chem. Int. Ed.*, 2018, **57**, 1792–1796.

112 C. S. Vogelsberg and M. A. Garcia-Garibay, *Chem. Soc. Rev.*, 2012, **41**, 1892–1910.

113 M. E. Howe and M. A. Garcia-Garibay, *J. Org. Chem.*, 2019, **84**, 9835–9849.

114 W. Danowski, T. van Leeuwen, S. Abdolahzadeh, D. Roke, W. R. Browne, S. J. Wezenberg and B. L. Feringa, *Nat. Nanotechnol.*, 2019, **14**, 488–494.

115 S. Krause and B. L. Feringa, *Nat. Rev. Chem.*, 2020, **4**, 550–562.

116 V. N. Vukotic, K. J. Harris, K. Zhu, R. W. Schurko and S. J. Loeb, *Nat. Chem.*, 2012, **4**, 456–460.

117 V. N. Vukotic, C. A. O'Keefe, K. Zhu, K. J. Harris, C. To, R. W. Schurko and S. J. Loeb, *J. Am. Chem. Soc.*, 2015, **137**, 9643–9651.

118 K. Zhu, V. N. Vukotic, C. A. O'Keefe, R. W. Schurko and S. J. Loeb, *J. Am. Chem. Soc.*, 2014, **136**, 7403–7409.

119 P. Martinez-Bulit, C. A. O'Keefe, K. Zhu, R. W. Schurko and S. J. Loeb, *Cryst. Growth Des.*, 2019, **19**, 5679–5685.

120 P. Li, N. A. Vermeulen, X. Gong, C. D. Malliakas, J. F. Stoddart, J. T. Hupp and O. K. Farha, *Angew. Chem. Int. Ed.*, 2016, **55**, 10358–10362.

121 Y. Song, A. E. Khudozhitkov, J. Lee, H. Kang, D. I. Kolokolov, A. G. Stepanov and M. Yoon, *Chem. Commun.*, 2020, **56**, 4468–4471.

122 R. Pallach, J. Keupp, K. Terlinden, L. Frentzel-Beyme, M. Kloß, A. Machalica, J. Kotschy, S. K. Vasa, P. A. Chater, C. Sternemann, M. T. Wharmby, R. Linser, R. Schmid and S. Henke, *Nat. Commun.*, 2021, **12**, 4097.

123 N. Farahani, K. Zhu, C. A. O'Keefe, R. W. Schurko and S. J. Loeb, *ChemPlusChem*, 2016, **81**, 836–841.

124 A. J. Stirk, B. H. Wilson, C. A. O'Keefe, H. Amarne, K. Zhu, R. W. Schurko and S. J. Loeb, *Nano Res.*, 2021, **14**, 417–422.

125 Z. Xiao, Y. Wang, S. Zhang, W. Fan, X. Xin, X. Pan, L. Zhang and D. Sun, *Cryst. Growth Des.*, 2017, **17**, 4084–4089.

126 S. M. Cohen, *Chem. Rev.*, 2012, **112**, 970–1000.

127 S.-Y. Chang, H. S. Kim, K. Chang and K.-S. Jeong, *Org. Lett.*, 2004, **6**, 181–184.

128 I. Yoon, D. Benítez, Y. L. Zhao, O. Š. Miljanić, S. Y. Kim, E. Tkatchouk, K. C. F. Leung, S. I. Khan, W. A. Goddard III and J. F. Stoddart, *Chem. - Eur. J.*, 2009, **15**, 1115–1122.

129 D. D. Günbaş and A. M. Brouwer, *J. Org. Chem.*, 2012, **77**, 5724–5735.

130 J. Berna, M. Alajarin, C. Marin-Rodriguez and C. Franco-Pujante, *Chem. Sci.*, 2012, **3**, 2314–2320.

131 A. Martinez-Cuezva, A. Saura-Sanmartin, T. Nicolas-Garcia, C. Navarro, R. A. Orenes, M. Alajarin and J. Berna, *Chem. Sci.*, 2017, **8**, 3775–3780.

132 D. A. Leigh, V. Marcos, T. Nalbantoglu, I. J. Vitorica-Yrezabal, F. T. Yasar and X. Zhu, *J. Am. Chem. Soc.*, 2017, **139**, 7104–7109.

133 A. Saura-Sanmartin, A. Martinez-Cuezva, A. Pastor, D. Bautista and J. Berna, *Org. Biomol. Chem.*, 2018, **16**, 6980–6987.

134 D. Sluysmans, P. Lussis, C. A. Fustin, A. Bertocco, D. A. Leigh and A. S. Duwez, *J. Am. Chem. Soc.*, 2021, **143**, 2348–2352.

135 Z. Cao, D. Wu, M. Li, F. Yang, Z. Li, W. An, S. Jiang, X. Zheng, C. Niu and D. Qu, *Chin. Chem. Lett.*, 2022, **33**, 1533–1536.

136 M. A. Olson, *Nat. Chem.*, 2015, **7**, 470–471.

137 K. Zhu, C. A. O'Keefe, V. N. Vukotic, R. W. Schurko and S. J. Loeb, *Nat. Chem.*, 2015, **7**, 514–519.

138 S. Yuan, L. Feng, K. Wang, J. Pang, M. Bosch, C. Lollar, Y. Sun, J. Qin, X. Yang, P. Zhang, Q. Wang, L. Zou, Y. Zhang, L. Zhang, Y. Fang, J. Li and H.-C. Zhou, *Adv. Mater.*, 2018, **30**, 1704303.

139 M. Ding, X. Cai and H. L. Jiang, *Chem. Sci.*, 2019, **10**, 10209–10230.

140 J. E. Mondloch, W. Bury, D. Fairen-Jimenez, S. Kwon, E. J. Demarco, M. H. Weston, A. A. Sarjeant, S. T. Nguyen, P. C. Stair, R. Q. Snurr, O. K. Farha and J. T. Hupp, *J. Am. Chem. Soc.*, 2013, **135**, 10294–10297.

141 A. Trabolsi, N. Khashab, A. C. Fahrenbach, D. C. Friedman, M. T. Colvin, K. K. Cotí, D. Benítez, E. Tkatchouk, J. C. Olsen, M. E. Belowich, R. Carmielli, H. A. Khatib, W. A. Goddard III, M. R. Wasielewski and J. F. Stoddart, *Nat. Chem.*, 2010, **2**, 42–49.

142 J. Berna, M. Alajarin and R. A. Orenes, *J. Am. Chem. Soc.*, 2010, **132**, 10741–10747.

143 A. Altieri, G. Bottari, F. Dehez, D. A. Leigh, J. K. Y. Wong and F. Zerbetto, *Angew. Chem. Int. Ed.*, 2003, **42**, 2296–2300.

144 A. Martinez-Cuezva, S. Valero-Moya, M. Alajarin and J. Berna, *Chem. Commun.*, 2015, **51**, 14501–14504.

145 K. Zhu, V. N. Vukotic and S. J. Loeb, *Chem. - Asian J.*, 2016, **11**, 3258–3266.

146 R. Arumugaperumal, M. Shellaiah, Y. K. Lai, P. Venkatesan, P. Raghunath, S. P. Wu, M. C. Lin, K. W. Sun, W. S. Chung and H. C. Lin, *J. Mater. Chem. C*, 2021, **9**, 3215–3228.

147 G. Gholami, B. H. Wilson, K. Zhu, C. A. O'Keefe, R. W. Schurko and S. J. Loeb, *Faraday Discuss.*, 2021, **225**, 358–370.

148 B. H. Wilson, L. M. Abdulla, R. W. Schurko and S. J. Loeb, *Chem. Sci.*, 2021, **12**, 3944–3951.

149 V. N. Vukotic, K. Zhu, G. Baggi and S. J. Loeb, *Angew. Chem. Int. Ed.*, 2017, **56**, 6136–6141.

150 K. Zhu, V. N. Vukotic and S. J. Loeb, *Angew. Chem. Int. Ed.*, 2012, **51**, 2168–2172.

151 L. Feng, Y. Qiu, Q.-H. Guo, Z. Chen, J. S. W. Seale, K. He, H. Wu, Y. Feng, O. K. Farha, R. D. Astumian and J. F. Stoddart, *Science*, 2021, **374**, 1215–1221.

152 L. Zhang, *Nat. Chem.*, 2022, **14**, 125–128.

153 C. Cheng, P. R. McGonigal, S. T. Schneebeli, H. Li, N. A. Vermeulen, C. Ke and J. F. Stoddart, *Nat. Nanotechnol. 2015 106*, 2015, **10**, 547–553.

154 A. Saura-Sanmartin, A. Martinez-Cuezva and J. Berna, *Chem*, 2021, **7**, 14–16.

155 B. H. Wilson, C. S. Vojvodin, G. Gholami, L. M. Abdulla, C. A. O'Keefe, R. W. Schurko and S. J. Loeb, *Chem*, 2021, **7**, 202–

211.
156 E. Escalante-Sánchez, B. Rodríguez-Molina and M. A. Garcia-Garibay, *J. Org. Chem.*, 2012, **77**, 7428–7434.
157 R. Arcos-Ramos, B. Rodriguez-Molina, E. Gonzalez-Rodriguez, P. I. Ramirez-Montes, M. E. Ochoa, R. Santillan, N. Farfán and M. A. Garcia-Garibay, *RSC Adv.*, 2015, **5**, 55201–55208.
158 S. Bracco, T. Miyano, M. Negroni, I. Bassanetti, L. Marchio, P. Sozzani, N. Tohnai and A. Comotti, *Chem. Commun.*, 2017, **53**, 7776–7779.
159 D. A. Leigh, V. Marcos and M. R. Wilson, *ACS Catal.*, 2014, **4**, 4490–4497.
160 A. Martinez-Cuezva, A. Saura-Sanmartin, M. Alajarin and J. Berna, *ACS Catal.*, 2020, **10**, 7719–7733.
161 A. W. Heard, J. M. Suárez and S. M. Goldup, *Nat. Rev. Chem.*, 2022, **6**, 182–196.
162 C. Kwamen and J. Niemeyer, *Chem. - Eur. J.*, 2021, **27**, 175–186.
163 J. M. Perez, J. Puigcerver, T. Orlando, A. Pastor, M. A. P. Martins, M. Alajarin, A. Martinez-Cuezva and J. Berna, *Org. Chem. Front.*, 2021, **8**, 4202–4210.
164 E. M. G. Jamieson, F. Modicom and S. M. Goldup, *Chem. Soc. Rev.*, 2018, **47**, 5266–5311.
165 J. R. J. Maynard and S. M. Goldup, *Chem*, 2020, **6**, 1914–1932.
166 A. De Juan, D. Lozano, A. W. Heard, M. A. Jinks, J. M. Suarez, G. J. Tizzard and S. M. Goldup, *Nat. Chem.*, 2022, **14**, 179–188.
167 K. M. Bąk, K. Porfyrakis, J. J. Davis and P. D. Beer, *Mater. Chem. Front.*, 2020, **4**, 1052–1073.
168 A. Martinez-Cuezva, C. Lopez-Leonardo, M. Alajarin and J. Berna, *Synlett*, 2019, **30**, 893–902.
169 T. Ogoshi, D. Kotera, S. Fa, S. Nishida, T. Kakuta, T. -a. Yamagishi and A. M. Brouwer, *Chem. Commun.*, 2020, **56**, 10871–10874.
170 J. Rotzel and M. Mayor, *Chem. Soc. Rev.*, 2013, **42**, 44–62.
171 Y. Wang, J. Sun, Z. Liu, M. S. Nassar, Y. Y. Botros and J. F. Stoddart, *Chem. Sci.*, 2017, **8**, 2562–2568.
172 A. Goujon, E. Moulin, G. Fuks and N. Giuseppone, *CCS Chem.*, 2019, **1**, 83–96.
173 A. Saura-Sanmartin, A. Pastor, A. Martinez-Cuezva and J. Berna, *Chem. Commun.*, 2022, **58**, 290–293.
174 C.-W. Chu, D. L. Stares and C. A. Schalley, *Chem. Commun.*, 2021, **57**, 12317–12320.
175 C. J. Bruns and J. F. Stoddart, *Acc. Chem. Res.*, 2014, **47**, 2186–2199.

